Received: 24 November 2025 | Revised: 29 April 2026 | Accepted: 4 May 2026

DOI: 10.1111/bph.70523

RESEARCH ARTICLE

Pharmacological activation of NO-cGMP signalling attenuates metabolic dysfunction-associated steatohepatitis

Krithika Rajeeth[1] | Malte Roessing[1] | Moritz Lehners[1] | Lisa Dietz[2] | Anja Schmitt[3] | Stephan Hailfinger[3] | Andreas Peter[4,5,6] | Leticia Quintanilla-Martinez[7,8] | Irene Gonzalez-Menendez[7,8] | Ingmar Mederacke[9] | German Ott[10,11] | Peter Sandner[2,12] | Matthias Schwab[11,13] | Robert Feil[1] | Susanne Feil[1]

[1]Interfaculty Institute of Biochemistry, University of Tübingen, Tübingen, Germany

[2]Cardiovascular Research, Pharma Research Centre, Bayer AG, Wuppertal, Germany

[3]Department of Medicine A, Hematology, Oncology, and Pneumology, University Hospital Münster, Münster, Germany

[4]Institute for Clinical Chemistry and Pathobiochemistry, University Hospital Tübingen, Tübingen, Germany

[5]Institute for Diabetes Research and Metabolic Diseases, Helmholtz Center Munich, University of Tübingen, Tübingen, Germany

[6]German Center for Diabetes Research (DZD e.V.), Neuherberg, Germany

[7]Department of Pathology and Neuropathology, University of Tübingen, Tübingen, Germany

[8]Cluster of Excellence iFIT (EXC2180) "Image-Guided and Functionally Instructed Tumor Therapies", University of Tübingen, Tübingen, Germany

[9]Department of Gastroenterology, Hepatology, Infectious Diseases and Endocrinology, Hannover Medical School, Hannover, Germany

[10]Department of Clinical Pathology, Robert Bosch Hospital, Stuttgart, Germany

[11]Dr. Margarete Fischer-Bosch Institute of Clinical Pharmacology, Bosch Health Campus, Stuttgart, Germany

[12]Department of Pharmacology, Hannover Medical School, Hannover, Germany

[13]Departments of Clinical Pharmacology and of Biochemistry and Pharmacy, University of Tübingen, Tübingen, Germany

Correspondence
Susanne Feil, Interfakultäres Institut für Biochemie, University of Tübingen, Auf der Morgenstelle 34, 72076 Tübingen, Germany.
Email: susanne.feil@uni-tuebingen.de

Funding information
This work was supported by grants from the EU Framework Program for Research and Innovation "Horizon 2020"–ERA-CVD JTC2017-044; the Deutsche Forschungsgemeinschaft (German Research Foundation) Projektnummer 335549539–GRK 2381, Projektnummer 434558229–INST 37/1133-1 FUGG, and FOR 2060 projects FE 438/5-2 and FE 438/6-2; and the Dr. K.H. Eberle Stiftung and Reinhard Frank

Background and Purpose: Metabolic dysfunction-associated steatohepatitis (MASH) is linked to activation of hepatic stellate cells (HSCs) to α-smooth muscle actin–positive myofibroblasts that produce collagen and proinflammatory cytokines. Quiescent HSCs express the NO-cGMP signalling axis. Modulating this pathway could alter HSC activation and fibrosis during MASH progression.

Experimental Approach: Using transgenic cGMP sensor mice, we monitored NO-induced cGMP in living HSCs. The relevance of this pathway was analyzed using HSC-specific mouse models, ApoE-deficient mice on high-fat diet as a MASH model, human liver sections, and published scRNA-seq datasets. For pharmacological activation of NO-cGMP signalling, BAY-543, an activator of NO-sensitive guanylyl cyclase (NO-GC) was used.

Abbreviations: Act, NO-CG activator BAY-543; ALT, alanine aminotransferase; ApoE KO, apolipoprotein E knockout; CFP, cyan fluorescent protein; cGi500, cGMP indicator with an apparent EC_{50} of 500 nM; cGKI, cGMP-dependent protein kinase type I; cGMP, 3′,5′-cyclic guanosine monophosphate; Col IV, Collagen IV; DEA-NO, diethylamine NONOate; FRET, Förster/fluorescence resonance energy transfer; HFD, high-fat diet; HSC, hepatic stellate cell; MASH, metabolic dysfunction-associated steatohepatitis; MASLD, metabolic dysfunction-associated steatotic liver disease; NO-GC, NO-sensitive guanylyl cyclase; PDE5, phosphodiesterase 5; SM22α, smooth muscle protein 22 alpha; SMA, α-smooth muscle actin; YFP, yellow fluorescent protein.

Stiftung. German Ott and Matthias Schwab were in parts supported by the Robert Bosch Stiftung, Stuttgart, Germany.

Key Results: HSCs in primary culture and liver tissue generated NO-induced cGMP and expressed NO-GC and cGMP-dependent protein kinase type I (cGKI). Compared to controls, HSC-specific cGKI knockout livers showed enhanced myofibroblast marker expression, indicating increased HSC activation and MASH susceptibility. MASH mice developed steatosis, fibrosis, and inflammation, and showed a high number of HSCs expressing NO-GC and cGKI. cGKI expression was also increased in human fibrotic livers as compared to healthy tissue. In MASH livers, oxidative stress could lead to reduced sensitivity of NO-GC to NO. Treatment of MASH mice with BAY-543, which targets oxidized/NO-insensitive NO-GC, significantly attenuated HSC activation, inflammation, collagen deposition, macro-steatosis, fibrosis, and serum liver enzymes.

Conclusion and Implications: The NO-cGMP-cGKI axis serves as both a functional pathway marker and regulator of HSCs. Pharmacological elevation of cGMP with an NO-GC activator represents a promising therapeutic strategy for MASH.

KEYWORDS

cGMP signalling, FRET imaging, Gucy, hepatic stellate cells, liver fibrosis, MASH, NO-GC activator, Prkg1

1 | INTRODUCTION

Metabolic dysfunction-associated steatotic liver disease (MASLD) (Rinella et al., 2024), formerly known as non-alcoholic fatty liver disease (NAFLD), is becoming highly prevalent worldwide. MASLD encompasses a spectrum of chronic liver diseases ranging from simple steatosis to metabolic dysfunction-associated steatohepatitis (MASH), which can progress to cirrhosis and hepatocellular carcinoma (Anstee et al., 2019). Hepatic stellate cells (HSCs) and their activated derivatives, often referred to as myofibroblasts, are unique mesenchymal cells of the liver that play a crucial role in the progression of MASH (Geng & Schwabe, 2025; Schwabe & Brenner, 2025). In their quiescent state, HSCs positively affect hepatocyte metabolism and regeneration (Sugimoto et al., 2025). During the process of chronic liver damage, they transform, losing their characteristic lipid droplets and adopting a fibroblast-like morphology with increased expression of α-smooth muscle actin (SMA), SM22α (also known as transgelin) and extracellular matrix components (Kisseleva & Brenner, 2021; Tsuchida & Friedman, 2017; Wiering et al., 2023; Yang et al., 2021). HSC activation dictates fibrosis development during MASH. Therefore, HSCs could act as potential targets for novel therapies for patients with fibrotic liver diseases.

The intracellular second messenger cyclic guanosine monophosphate (**cGMP**) is important to many physiological processes (Beavo & Brunton, 2002; Hofmann, 2020). It is generated from GTP by membrane-associated guanylyl cyclases such as **GC-A** or **GC-B**, or by the cytosolic nitric oxide (**NO**)–sensitive guanylyl cyclase (**NO-GC**, also known as soluble guanylyl cyclase, sGC) (Feil & Kemp-Harper, 2006; Lucas et al., 2000). NO-GC is activated by binding of NO, which is generated by three types of NO synthases (**NOS**): neuronal NOS (**nNOS or NOS1**), inducible NOS (**iNOS or NOS2**) and endothelial NOS (**eNOS or NOS3**) (Forstermann & Sessa, 2012). The NO-GC is a heterodimeric enzyme formed from an α1 or α2 subunit and a β1 subunit containing the NO-binding haem cofactor. The α1β1 dimer is the major isoform in most tissues (Derbyshire & Marletta, 2012; Friebe &

What is already known?

- Hepatic stellate cells (HSCs) play a crucial role in metabolic dysfunction-associated steatohepatitis (MASH).
- Oxidative stress in MASH might impair cGMP generation by NO-sensitive guanylyl cyclase (NO-GC) in HSCs.

What does this study add?

- The NO-cGMP axis is a marker of quiescent and activated HSCs in the liver.
- BAY-543, which targets oxidized/NO-insensitive NO-GC, improves MASH in mice.

What is the clinical significance?

- Targeting HSCs with the NO-GC activator BAY-543 could improve MASH treatment in humans.

Koesling, 2003). cGMP's downstream effects are mainly mediated by cGMP-dependent protein kinases (**cGKs**) (Feil et al., 2003). The two known cGKs in mammals are the cytosolic cGMP-dependent protein kinase type I (**cGKI; also known as protein kinase G1, PKG1**) and the plasma membrane-anchored **cGMP-dependent protein kinase type II**. To terminate the signal, cGMP is hydrolyzed by phosphodiesterases (**PDEs**) (Bender & Beavo, 2006). In the healthy liver, the cGMP generator **NO-GC** (He et al., 2023; Theilig et al., 2001; Yang et al., 2021) and its downstream effector cGKI (Lutz et al., 2011) are expressed in HSCs. The cGMP axis has been linked to HSCs in their resting state (He et al., 2023). Its function in activated HSCs in the context of liver diseases is not well understood (Kelly et al., 2025).

Chronic liver diseases like MASH are associated with oxidative stress, which potentially contributes to disease progression through impairment of NO-cGMP signalling in HSCs. First, oxidative stress might lead to reduced bioavailability of NO inside the liver (Wiest & Groszmann, 2002). Conversely, NO production in the peripheral systemic circulation is increased, leading to vascular disturbances in liver cirrhosis (Kreisel et al., 2021). Second, under oxidative stress conditions, the haem group in NO-GC may become oxidized and eventually lost, resulting in an NO-insensitive enzyme (Stasch et al., 2015). A variety of drugs that enhance NO-GC activity have been developed, namely, NO-GC stimulators (also known as soluble guanylyl cyclase [sGC] stimulators) and NO-GC activators (also known as soluble guanylyl cyclase [sGC] activators) (Sandner et al., 2021). Although stimulators act not only independently of NO but also synergistically when NO is bound to NO-GC, the group of activators can bind to the unoccupied haem-binding pocket of oxidized NO-GC (Dai & Stuehr, 2025; Sandner et al., 2021). It is therefore assumed that NO-GC activators increase the availability of cGMP, particularly in diseased tissues that exhibit oxidative stress, whereas NO-GC stimulators are less effective under oxidative conditions.

Preclinical studies have shown that NO-GC stimulators improve liver health in some models of liver cirrhosis (Kreisel et al., 2021). However, it cannot be excluded that NO-GC stimulators can also function independently of NO-GC and cGMP signalling (P. J. Chen et al., 2020). Research into the therapeutic potential of NO-GC activators, which are expected to target oxidized NO-GC associated with the progression of liver disease, is limited. Some studies with NO-GC activators have been conducted on models with severe fibrosis/cirrhosis using male rats, with steatosis not being taken into account (Brusilovskaya et al., 2020; Jones et al., 2023; Knorr et al., 2008). Since fibrosis is closely linked to metabolic-associated diseases and steatosis (Jamialahmadi et al., 2024; Raverdy et al., 2024), we used the apolipoprotein E knockout (ApoE KO) mouse model for the investigation of MASH. The absence of ApoE is known to induce metabolic syndrome, characterized by dyslipidaemia, obesity and atherosclerosis (Zhang et al., 1992). Combined with a high-fat diet (HFD), ApoE KO mice can be used to study MASH with steatosis, fibrosis and inflammation (Camargo et al., 2022; Schierwagen et al., 2015).

In the present study, we investigated the functional relevance of NO-cGMP signalling in MASH by combining real-time imaging of cGMP in HSCs with the analysis of mouse models and human MASH livers and testing the effects of pharmacological intervention with an NO-GC activator. Our focus was on the NO-NO-GC-cGMP-cGKI axis in activated HSCs and on the therapeutic potential of the potent and selective NO-GC activator BAY-543 (Stehle et al., 2022; Wittrien et al., 2025).

2 | METHODS

2.1 | Animals

Primary HSCs were isolated from wild-type or transgenic cGMP sensor mice on a C57BL/6 background. Livers for cGMP imaging were also isolated from cGMP sensor mice. cGi500-L1 mice express the Förster/fluorescence resonance energy transfer (FRET)–based cGMP sensor cGi500 globally in all cell types (B6-Gt (ROSA)26Sor<tm4.1 (ACTB-tdTomato,-cGi-500)Feil>, genotype: cGi500$^{+/L1}$) (Thunemann et al., 2013). Mice with HSC-specific expression of the cGMP sensor (B6;Tg (Lrat-cre)1<Rshw>; B6;129-Gt (ROSA)26Sor<tm4(ACTB-tdTomato,-cGi-500)Feil>, genotype: Lrat-Cre$^{Cre/+}$; cGi500$^{+/L2}$) or of the red tdTomato reporter Ai9 (Madisen et al., 2010) (genotype: Lrat-Cre$^{Cre/+}$; Ai9$^{+/L2}$) were generated via Cre/loxP recombination using female Lecithin retinol acyltransferase (Lrat)–Cre mice (Mederacke et al., 2015). Mice with a HSC-specific deletion of cGKI (HSC-cGKI-KO, genotype: Lrat-Cre$^{Cre/+}$; cGKI$^{L1/L2}$) were generated by crossing a loxP-flanked cGKI mouse line (B6.129-Prkg1<tm2Naw>) (Wegener et al., 2002) with Lrat-Cre mice. HSC-cGKI-KO animals were compared with litter-matched control mice (controls, genotype: Lrat-Cre$^{+/+}$; cGKI$^{+/L2}$). To analyse MASH, we used male and female ApoE KO mice (B6.129P2-Apoe<tm1Unc>, genotype: ApoE$^{-/-}$) (Zhang et al., 1992) and litter-matched controls (genotype: ApoE$^{+/-}$). The controls were fed a normal diet (Altromin Spezialfutter GmbH & Co. KG, Lage, Germany) and compared with ApoE KO fed a HFD as previously described (Camargo et al., 2022; Schierwagen et al., 2015), with a modification of the HFD (21% butter fat and 1.25% cholesterol, Ssniff Spezialdiäten GmbH, Soest, Germany), feeding duration from 7 to 18 weeks starting at 10–14 weeks of age. Another group of litter-matched ApoE KO mice was fed the HFD supplemented with the NO-GC activator BAY-543 (150 ppm or 150 mg·kg^{-1} diet; provided by Bayer AG, Wuppertal, Germany) for 18 weeks. BAY-543 is a potent and selective NO-GC activator as described previously (Stehle et al., 2022).

All animal experiments were conducted in accordance with the Directive 2010/63/EU of the European Parliament and the German legislation of the Animal Welfare Act, with authorization of the local Ethics Committee for Animal Research (Regierungspräsidium Tübingen). Animal studies are reported in compliance with the ARRIVE guidelines (Percie et al., 2020) and with the recommendations made by the British Journal of Pharmacology (Lilley et al., 2020).

All animals were kept on a 12-h/12-h light/dark cycle and had access to regular chow or HFD ad libitum. Mice were genotyped at 3 weeks of age and at the end of the experiment if required.

2.2 | Isolation of hepatic stellate cells (HSCs) from mouse liver

Mice were killed using CO_2 followed by permanent cessation of the circulation. For isolation of primary HSCs from murine liver (C57BL/6 background) the inferior vena cava was cannulated followed by a two-step perfusion protocol as previously described (Mederacke et al., 2015), with a minor reduction of the digestion time from 25 to 20 min. Primary HSCs were cultured for up to 8 days in full medium (Dulbecco's Modified Eagle Medium [DMEM] with 10% fetal bovine serum [FBS] and penicillin/streptomycin) at 37°C and 6% CO_2.

2.3 | cGMP/FRET imaging

For cGMP imaging of HSCs in vitro, primary cultures were prepared from cGi500 sensor mice. HSCs were grown on 12-mm glass coverslips in full medium and imaged using an epifluorescence microscope as described for vascular smooth muscle cells (Lehners et al., 2025). Ex vivo cGMP imaging of whole liver tissue from HSC-specific cGMP sensor mice was performed using a confocal spinning disk microscope (Visitron, Puchheim, Germany) controlled by the VisiView® software (Visitron). Microscopic equipment and camera were used as described (Lehners et al., 2025). The imaging chamber RC-26 (#64-0234, Warner Instruments, Holliston, USA) was sealed with a 24 × 40 mm coverslip. Liver tissue was fixed in the superfusion chamber using a slice hold-down (SHD-26H/10, Warner Instruments). During cGMP/FRET imaging, the liver pieces were constantly superfused with imaging buffer (Lehners et al., 2025) or imaging buffer with drugs at a flow rate of 60 ml·h^{-1}. Imaging was performed at 0.2 Hz with a gain of 500 without binning at room temperature. After the measurement, the recorded region was documented at high resolution by acquisition of Z-stacks.

2.4 | Offline analysis of cGMP/FRET measurements

Images acquired during measurements were processed using Fiji (Schindelin et al., 2012) to determine the mean fluorescence intensity of regions of interest (ROIs). To minimize the disturbing effects of tissue movement over time, images were aligned using the MultiStackReg plugin in Fiji before extracting fluorescence intensities. cGMP/FRET signals were calculated in MS Excel (Microsoft Corporation) and further analysed with OriginPro software (OriginLab Corporation). Background correction was applied to the CFP and YFP emission values by subtracting the mean fluorescence intensity of a cell-free region. The cGMP/FRET signals, represented by the CFP/YFP ratio ($R \sim [cGMP]$), were then calculated and normalized to the baseline, which was defined as the first 20–30 frames of each measurement. Changes in the ratio traces were considered indicative of cGMP changes if the CFP and YFP channels exhibited antiparallel movements. Signals that did not show antiparallel movement, for example, due to focus drift in ex vivo measurements, were excluded from analysis.

2.5 | Analysis of metabolic dysfunction-associated steatohepatitis (MASH) mice

After 18 weeks of HFD, the mice were killed for tissue and blood collection using anaesthesia with 5% isoflurane and decapitation. The liver tissue was weighed, and pieces from left lateral, left medial, right lateral, right medial and caudate lobes were prepared for further analysis (Fiebig et al., 2012). Liver samples were either snap-frozen in liquid nitrogen and stored at −80°C for Western blot analysis (right lateral lobe), RNA isolation (caudate lobe) and biochemical analysis (left medial lobe) or fixed in 4% paraformaldehyde for 3 h and embedded in paraffin or Tissue Tek for the preparation of tissue sections (left lateral and right medial lobes). Whole blood for the determination of BAY-543 concentration was collected in EDTA microtubes (Sarstedt, Nuembrecht, Germany). Blood for the determination of alanine aminotransferase and lipid levels was collected in Lithium-Heparin microtubes (Sarstedt). Blood samples were centrifuged at 3000*g* for 10 min at 4°C, and then, the supernatant was stored at −80°C. Bay-543 concentration was analysed by LCMS/MS (Bayer AG, Wuppertal, Germany). Cholesterol, high-density lipoprotein, low-density lipoprotein, triglycerides and alanine aminotransferase in plasma and cholesterol and triglycerides in liver tissue, homogenized in PBS containing 1% Triton X-100, were determined on an Atellica Solution clinical chemistry analyser (Siemens Healthineers, Erlangen, Germany).

Blood pressure measurement was performed in male and female mice using the non-invasive CODA® tail-cuff system (Kent Scientific, Torrington, USA) at the end of the feeding period. Data of three consecutive days were averaged for each animal.

2.6 | Histological and immunohistochemical staining

Formalin-fixed paraffin-embedded tissue sections (10 µm) were stained with haematoxylin and eosin. To detect collagen fibre accumulation, the sections were first stained with 0.02% FG solution (Fast Green FCF Dye Content; Merck, Darmstadt, Germany) for 15 min in distilled water, followed by a counterstaining with picrosirius red solution, a mixture of 0.05% Sirius red (Direct Red 80; Sigma-Aldrich) and 0.02% fast green in picric acid for 1 h. The sections were briefly washed in water, dehydrated and mounted in DPX mounting medium (Sigma-Aldrich, St. Louis, USA). The staining procedure was adapted and modified from Segnani et al. (2015). Immunohistochemical staining was done using the avidin–biotin complex method and diaminobenzidine as a chromogen (Vector Laboratories, Newark, USA). Serial sections of the left lateral lobe were analysed using antibodies against cGKI (homemade) (Valtcheva et al., 2009), SMA (ab124964; Abcam, Cambridge, USA, RRID:AB_11129103) or Mac-2 (also named galectin

3, CL8942; Cedarlane, Burlington, Canada, RRID:AB_10060424). Stained sections were mounted in Aquatex (VWR, Radnor, USA).

2.7 | Immunofluorescence staining

Immunofluorescence staining was performed on frozen liver sections from right medial lobes (10 μm) and cultured primary HSCs. The sections were incubated with primary antibodies against SMA (ab124964; Abcam, RRID:AB_11129103), cGKI (homemade; Valtcheva et al., 2009), the β_1 subunit of NO-GC (GUCY1B3, ab24824; Abcam, RRID:AB_448398), collagen IV (ab6586; Abcam, RRID:AB_305584) or desmin (MA5-33065; Thermo Fisher Scientific, Waltham, USA, RRID:AB_2810158). As secondary antibodies, goat anti-rabbit Alexa 488 (A11008; Life Technologies, Carlsbad, USA, RRID:AB_143165) or goat anti-rabbit Alexa 555 (A21428; Life Technologies, RRID:AB_141784) were used. For co-staining, sections that were first stained for NO-GC or cGKI were additionally incubated with anti-desmin Alexa 488 (ab185033; Abcam, RRID:AB_2892748). Finally, the sections were mounted in DAPI-containing mounting medium (ROTI®Mount FluorCare DAPI, Roth, Karlsruhe, Germany). Primary HSCs isolated from mouse liver and cultured on 12-mm glass coverslips were fixed with 3.7% formaldehyde on Day 2 or Day 8. The cells were stained with the same antibodies as for liver sections detecting desmin, the β_1 subunit of NO-GC, cGKI or SMA, followed by a goat anti-rabbit Alexa 488 secondary antibody and nuclear staining with DAPI-containing mounting medium (ROTI®Mount FluorCare DAPI, Roth).

2.8 | Image analysis

Histochemical staining was documented using an upright microscope (Axioskop 20, Zeiss, Oberkochen, Germany) equipped with an A-Plan 10×/0.5 and a Plan NeoFluar 20×/0.5 objectives (Zeiss), an EOS 750 D (Canon) digital camera and the EOS utility software. Images were documented in brightfield. Sections that were stained with haematoxylin and eosin and picrosirius red/fast green were additionally scanned with a Ventana DP200 (Roche, Basel, Switzerland) and processed with the Image Viewer MFC Application. Final image preparation was performed with Fiji. Immunofluorescent images were acquired using a confocal laser scanning microscope (LSM 710 or LSM 980, Zeiss) with a 20× objective. The images were documented using the ZEN Black or ZEN Blue software (Zeiss).

The histopathological analysis of haematoxylin and eosin and picrosirius red/fast green–stained liver sections was performed by an experienced pathologist following the Ishak score (Ishak et al., 1995) and considering also MASH histopathological features such as macro- and micro-steatosis, ballooning and inflammation. Quantification of picrosirius red-positive and immunohistochemically stained areas was performed using Fiji. Immunofluorescence images were analysed using QuPath (version v0.4.3 from qupath.github.io) (Bankhead et al., 2017). The image analysis was adapted from an online tutorial titled 'Introduction to QuPath for Multiplexed Fluorescence Microscopy' by the Bioimage Informatics Facility.

2.9 | Human liver sections

Formalin-fixed paraffin-embedded tissues from patients diagnosed with liver fibrosis due to cholelithiasis and cirrhosis due to steatosis with unclarified cause were provided by the Department of Clinical Pathology, Robert Bosch Hospital, Stuttgart, Germany. The use of biomaterial has been approved by the ethics committee of the Medical Faculty, University Tübingen, Germany (ethical approval number: 287/2025 BO2). The tissues, which have been anonymized, were cut in serial sections (10 μm) and used for picrosirius red/fast green staining or immunostaining.

2.10 | Inspection of published human liver scRNA-seq datasets

To analyse the mRNA expression of cGMP pathway genes in human liver cells, the Single Cell Portal was searched for relevant published single-cell RNA sequencing (scRNA-seq) datasets. In the human liver fibrosis scRNA-seq atlas (accession number SCP2154), presented by Fabre and colleagues (2023), data from multiple studies have been integrated (GSE185477, GSE125188, GSE156625, GSE192740, GSE115469, GSE136103). We analysed genes associated with the cGMP pathway (Figure 4d,e) to create a dot plot or UMAPs representing the mRNA expression of these genes in each cell cluster. mRNA expression was normalized across all cell types that were present in the respective sample.

2.11 | Quantitative RT-PCR

RNA was isolated from snap-frozen liver samples using the RNeasy mini kit (#74106, Qiagen, Venlo, Netherlands) according to the manufacturer's instructions. Subsequently, RNA was transcribed into cDNA with the Biozym cDNA synthesis kit (Biozym, Hessisch Oldendorf, Germany) using random hexamer primers according to the manufacturer's protocol. Transcript levels were quantified using the Green-MasterMix (Genaxxon, Ulm, Germany) and the QIAquant 384 system (Qiagen). Relative transcript expression was calculated with the 2 (−ΔΔCt) method. Glyceraldehyde 3-phosphate dehydrogenase (*Gapdh*) was used as a reference gene. Primer sequences used for qPCR: *Gapdh*: fw, ACCATCTTCCAGGAGCGAGA, rev, GGCGGAGATGATGACCCT; *Acta2*: fw, TGCCCAGACATCAGGGAGTAA, rev, TCGGATACTTCAGCGTCAGGA; *Ccl2*: fw, ACTCATTCACCAGCAAG, rev, TTGAGCTTGGTGACAAAAACT; *Cxcl10*: fw, TCATCCTGCTGGGTCTGAGTGG, rev, CTCATCATTCTTTTTCATCGT; *Il1b*: fw, GTGTCTTTCCCGTGGACCTT, rev, TCGTTGCTTGGTTCTCCTTG; *Infg*: fw, CTTCTTCAGCAACAGCAAGGCGAAA, rev, CATTGAATG CTTGGCGCTGGA.

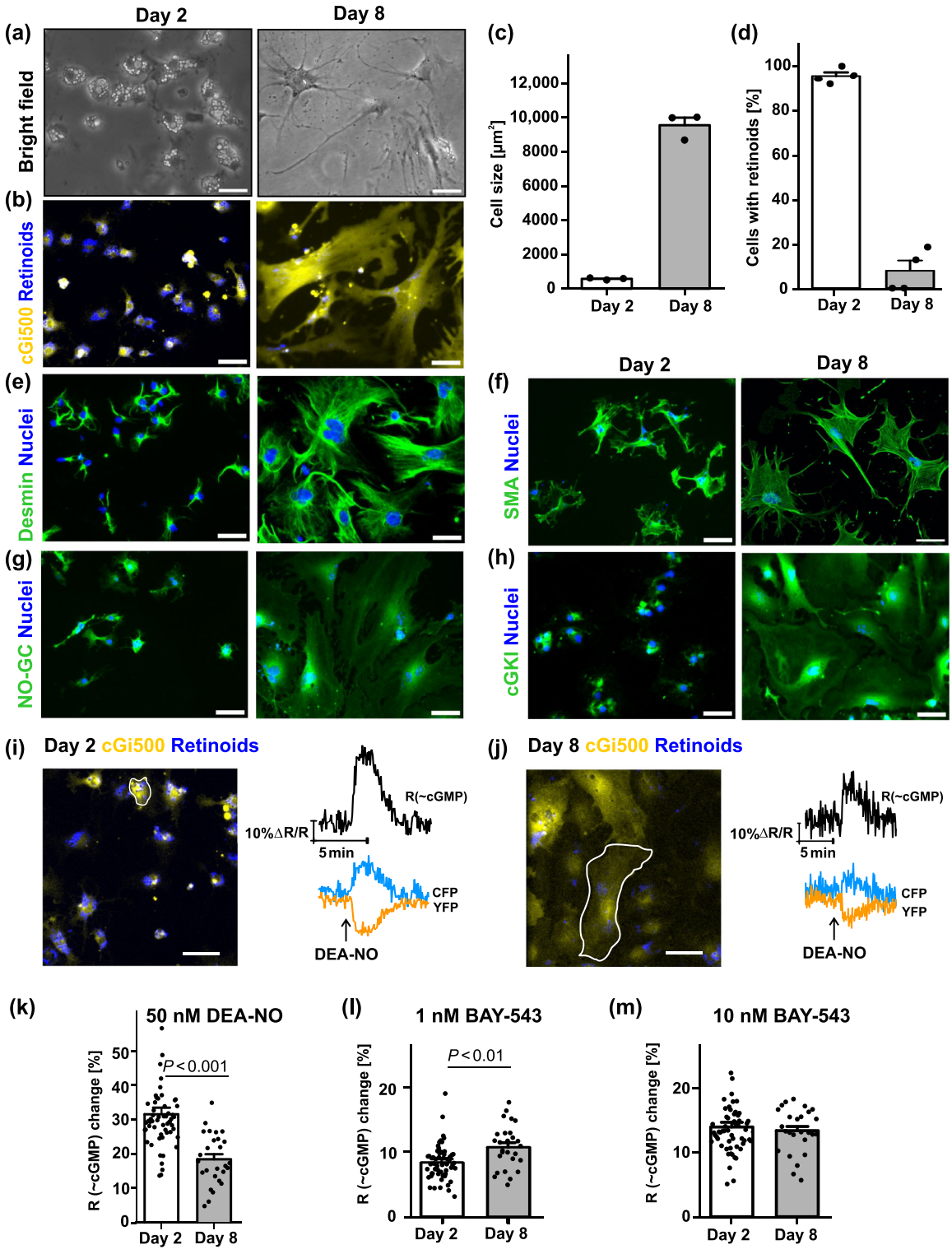

FIGURE 1 Legend on next page.

2.12 | Western blot analysis

Protein was extracted from snap-frozen liver tissues using a lysis buffer (50 mM Tris-Cl, 100 mM NaCl, 5 mM EDTA, 2% w/v SDS, 2.5mM PMSF) and a FastPrep-24 device (MP Biomedicals, Eschwege, Germany). The protein concentration was determined using Pierce™ BCA Protein Assay Kit (REF 23227; Thermo Scientific) according to the manufacturer's instructions. For Western blot analysis, primary antibodies against the β_1 subunit of NO-GC (GUCY1B3; ab24824; Abcam, RRID:AB_448398), cGKI (homemade) (Valtcheva et al., 2009), SM22α (ab14106; Abcam, RRID:AB_443021) and GAPDH (2118; Cell Signalling, RRID:AB_561053) were used. Secondary antibodies were horseradish peroxidase-conjugated IgG (7074; Cell Signalling, RRID:AB_2099233). The Immunorelated procedures used comply with the recommendations made by the *British Journal of Pharmacology* (Alexander et al., 2018).

2.13 | Statistics

Statistical analysis of data was performed using OriginPro (version 9.8.5.201, OriginLab Corporation). Data are represented as mean ± SEM. The Shapiro–Wilk test was used to test the normal distribution of the data. The Mann–Whitney *U*-test was performed for pairwise comparison of non-normally distributed data. A two-sample *t*-test was used for pairwise comparison of normally distributed data. $P < 0.05$ was considered statistically significant.

2.14 | Data and analysis

This manuscript complies with the recommendations and requirements of the *British Journal of Pharmacology* on experimental design and analysis (Curtis et al., 2025).

2.15 | Nomenclature of targets and ligands

Key protein targets and ligands in this article are hyperlinked to corresponding entries in the IUPHAR/BPS Guide to PHARMACOLOGY http://www.guidetopharmacology.org and are permanently archived in the Concise Guide to PHARMACOLOGY 2025/26 (Alexander, Fabbro, Gibb, et al., 2025, Alexander, Fabbro, Peach, et al., 2025; Alexander, Gibb et al., 2025).

3 | RESULTS

3.1 | Primary murine hepatic stellate cells (HSCs) in culture show functional NO-cGMP signalling

Primary HSCs were isolated from the livers of healthy mice and cultured for a period of up to 8 days. After 2 days in culture, HSCs started to develop tiny processes and displayed a star-shaped morphology together with retinoid-containing lipid droplets visualized by the blue autofluorescence of retinoids (Figure 1a left, b left). After 8 days in culture, the HSCs were larger with numerous processes and fewer lipid droplets compared with Day 2, consistent with an activated myofibroblast-like phenotype (Figure 1a right, b right,c,d). The average size of HSCs increased almost 20-fold, from 575 ± 35 μm^2 on Day 2 to 9557 ± 358 μm^2 on Day 8 (Figure 1c). From Day 2 to Day 8 in culture, the fraction of HSCs with retinoids decreased from 94% ± 2% to 8% ± 5% (Figure 1d). Antibody staining of HSCs showed that the cultured cells on Day 2 and Day 8 were positive for desmin, a marker of murine HSCs (Yokoi et al., 1984) (Figure 1e). Additionally, the cells expressed SMA (Figure 1f), the cGMP generator NO-GC (Figure 1g) and the cGMP downstream effector cGKI (Figure 1h) on Day 2 and Day 8.

For real-time imaging of cGMP in living HSCs, we isolated the cells from transgenic cGMP sensor mice expressing the FRET-based cGMP sensor cGi500 globally in all cell types (cGi500 mice) and analysed them using an epifluorescence microscope (Thunemann et al., 2013). Note that the yellow fluorescence of the cells (Figure 1b) indicates sensor expression but not the intracellular cGMP concentration. The cGMP concentration is reflected by CFP/YFP ratio curves recorded by FRET microscopy (Figure 1i,j). Superfusion of the cultured HSCs with the NO donor DEA-NO (50 nM) triggered robust cGMP elevations in both Day 2 and Day 8 HSCs (Figure 1i,j, black traces). However, the NO-induced cGMP response was significantly diminished in Day 8 HSCs versus Day 2 HSCs, as evidenced by a reduced peak height (Figure 1k). This suggested a decrease in NO-GC activity in activated HSCs on Day 8, possibly due to increased oxidative stress affecting the cells during prolonged cell culture. Next, we exposed the HSCs to the NO-GC activator BAY-543, which activates forms of NO-GC that are unresponsive to NO and can occur under oxidative stress disease conditions (Dai & Stuehr, 2025). BAY-543 (1 nM, 10 nM) induced cGMP signals in HSCs in a concentration-dependent manner and, unlike

FIGURE 1 cGMP signalling in primary mouse hepatic stellate cells (HSCs) cultured for 2 and 8 days. (a) Brightfield images of wild-type HSCs. (b) Visualization of retinoids by their autofluorescence (blue) in cGi500 expressing HSCs (yellow) isolated from cGMP sensor mice. (c) Cell size on Day 2 (50 cells from 3 coverslips) and Day 8 (71 cells from 3 coverslips). (d) Percentage of cells with retinoids on Day 2 (260 cells from 4 coverslips) and Day 8 (46 cells from 4 coverslips). (e–h) Immunofluorescence staining of HSCs on Day 2 and Day 8 for (e) desmin, (f) SMA, (g) NO-GC and (h) cGKI (i–j) real-time cGMP imaging in HSCs expressing the cGMP sensor cGi500. Representative image of (i) Day 2 HSCs and (j) Day 8 HSCs expressing cGi500 (yellow). Retinoids are blue. The ratio of cyan fluorescent protein (CFP, cyan trace) emission over yellow fluorescent protein (YFP, yellow trace) emission indicates the intracellular cGMP concentration (ΔR/R, black trace) in the cells outlined in white. Administration of DEA-NO (50 nM) is indicated by a black arrow. (k–m) Analysis of the cGMP increases (peak heights) in response to (k) 50 nM DEA-NO, (l) 1 nM BAY-543, (m) 10 nM BAY-543 in Day 2 HSCs ($n = 57$ cells) and Day 8 HSCs ($n = 27$ cells). Data are represented as mean ± SEM. *P*-values obtained with the Mann–Whitney *U*-test (k–m) are indicated. Scale bars, 50 μm. DEA-NO, diethylamine NONOate.

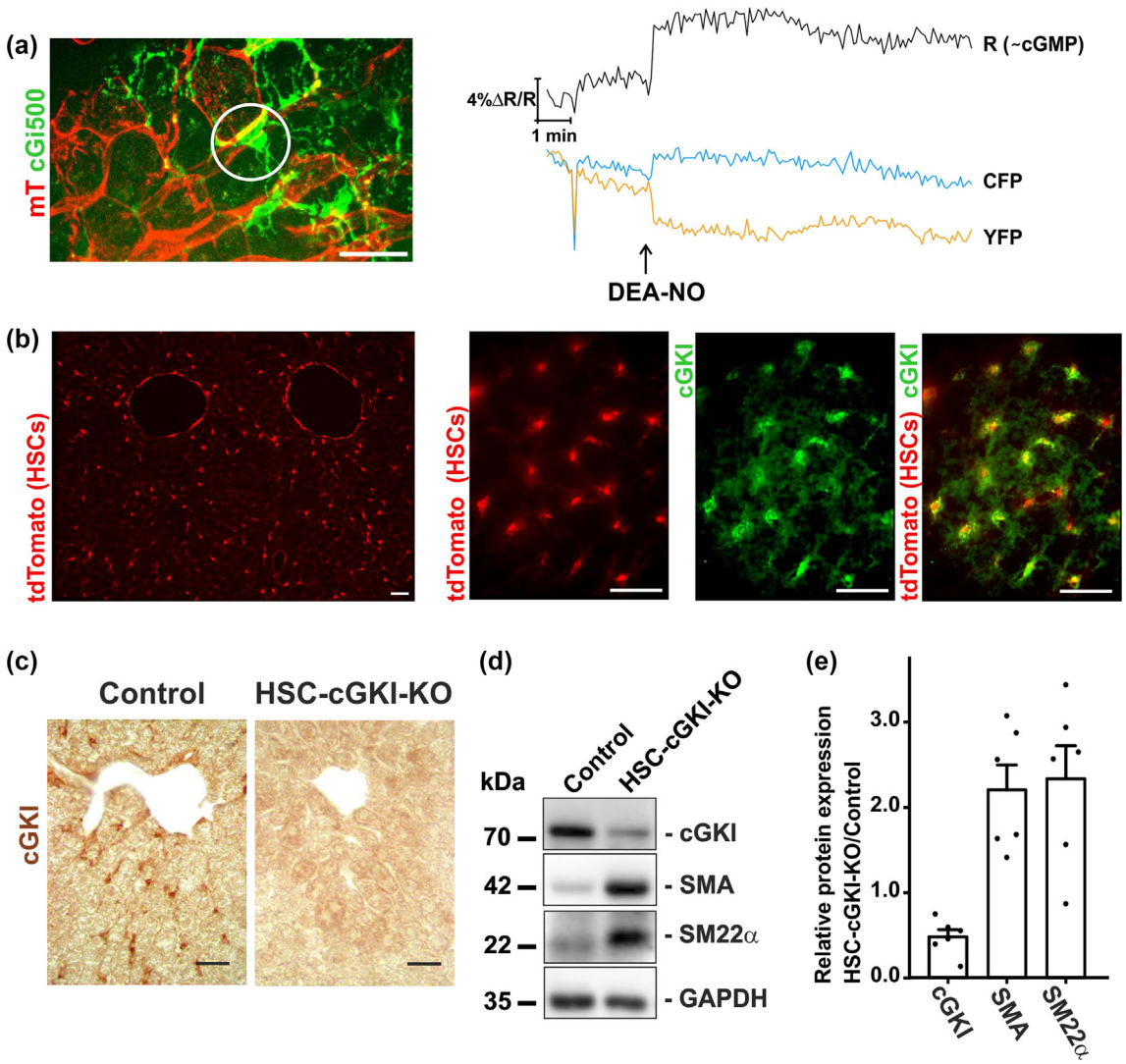

FIGURE 2 cGMP signalling in hepatic stellate cells (HSCs) within the mouse liver. (a) Expression of the cGMP sensor cGi500 (green) in HSCs of a whole-mount liver preparation isolated from HSC-specific cGMP sensor mice. HSCs (green) and non-HSCs (red) express cGi500 in the cytosol and the red fluorescent tomato protein in the membrane (mT), respectively. The cGMP/FRET ratio ($\Delta R/R$ [~cGMP], black trace) shows the cGMP concentration in the HSC outlined in white. Cyan fluorescent protein (CFP) and yellow fluorescent protein (YFP) fluorescence of the sensor are shown in cyan and yellow, respectively. Administration of DEA-NO (100 μM) is indicated by the black arrow. The data is representative of $n = 3$ experiments. (b) Liver sections of HSC-specific red fluorescent protein (tdTomato) reporter mice expressing tdTomato (red, detected without further antibody staining) in HSCs, and immunofluorescence staining of the sections for cGKI (green). The data are representative of livers from $n = 3$ animals. (c) Liver sections of 20-week-old control and litter-matched HSC-specific cGKI knockout mice (HSC-cGKI-KO) stained for cGKI (brown). The data are representative of livers from $n = 4$ animals each. (d) Representative Western blot and (e) quantification of cGKI, SMA and SM22α expression in 91-week-old HSC-cGKI-KO mice ($n = 6$) in relation to the corresponding litter-matched control mice ($n = 6$). Scale bars, 50 μm. DEA-NO, diethylamine NONOate; mT, membrane tomato.

DEA-NO, cGMP signals were not reduced in Day 8 versus Day 2 (Figure 1l,m).

Together, these findings indicated that culturing HSCs for 8 days resulted in their activation to a myofibroblast-like phenotype. The cultured HSCs expressed a functional NO-cGMP axis, the activity of which was reduced in the activated cell state. Interestingly, in contrast to NO, cGMP responses to BAY-543 did not decrease with HSC activation.

3.2 | Hepatic stellate cells (HSCs) in liver tissue show functional NO-cGMP signalling influencing HSC activation in vivo

To investigate cGMP signalling selectively in HSCs in the native liver, we generated HSC-specific cGMP sensor mice via Cre/loxP-mediated expression of the cGMP sensor cGi500. Lrat-Cre mice, which are reported to excise loxP-flanked DNA in desmin-positive HSCs

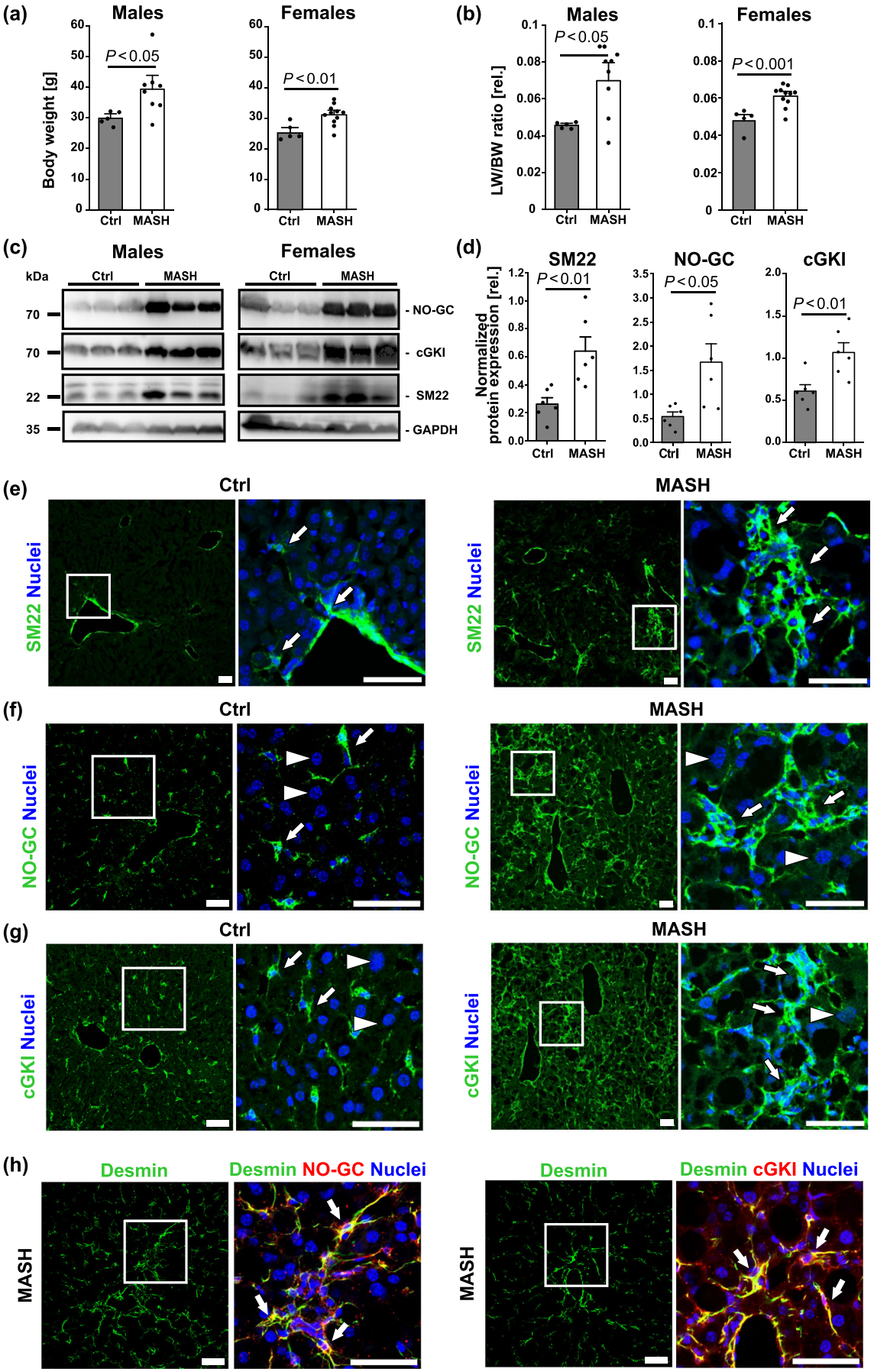

FIGURE 3 Legend on next page.

(Mederacke et al., 2013), were crossed with a 'floxed' cGMP sensor mouse line containing a loxP-flanked stop sequence (mT/cGi500 mice) (Thunemann et al., 2013). As shown in Figure 2a (left), whole-mount liver preparations from the HSC-specific cGMP sensor mice demonstrated sensor expression in cells with HSC-typical branching (cGi500, green), whereas nonrecombined cells expressed the red fluorescent tomato protein in the plasma membrane (mT, red). Importantly, real-time in situ cGMP imaging of sensor-expressing HSCs in acutely isolated liver tissue demonstrated an increase in cGMP in response to NO application (Figure 2a right, black trace). These data indicated the presence of a functional NO-cGMP signalling pathway in HSCs under physiological conditions in vivo.

To analyse the expression of the cGMP effector cGKI, we genetically labelled HSCs with red fluorescent protein (tdTomato, distributed throughout the cells) by crossing Lrat-Cre mice with the tdTomato-expressing Ai9 reporter line. Liver sections from these mice showed HSC-specific expression of tdTomato (Figure 2b) as previously described (Mederacke et al., 2013). Staining of these sections with an antibody against cGKI revealed that most HSCs expressed cGKI (Figure 2b right panels, overlay red/green). cGKI was not detectable in other cell types of the liver except vascular smooth muscle cells of blood vessels (Figure 2b, and data not shown). These findings confirmed previous data suggesting that cGKI could serve as an alternative marker for HSCs in healthy liver (Lutz et al., 2011), in addition to conventional lineage/activation markers.

To explore the function of cGKI-mediated cGMP signalling in HSCs, we generated HSC-specific cGKI knockout mice (HSC-cGKI-KO mice) by crossing the Lrat-Cre mouse line to a mouse line carrying a loxP-flanked allele of the cGKI gene. Immunohistochemistry staining of liver sections from 20-week-old HSC-cGKI-KO versus litter-matched controls showed a marked reduction of cGKI protein in HSCs (Figure 2c). The HSC-cGKI-KO mice appeared healthy and displayed no obvious defects up to 2 years of age. Livers from aged HSC-cGKI-KO mice ($n = 6$; average age 91 weeks) were compared with those of litter-matched controls ($n = 6$). The strong reduction of cGKI protein level in liver tissue of the HSC-cGKI-KO mice was confirmed by Western blot analysis (Figure 2d,e). The residual amount of cGKI detected in the livers of the aged HSC-cGKI-KO mice may have resulted from incomplete cGKI deletion in a fraction of HSCs or from cGKI expression in non-HSCs, such as vascular smooth muscle cells or fibroblasts. Interestingly, expression of the HSC activation markers SMA and SM22α was strongly increased in HSC-cGKI-KO livers compared with litter-matched controls (Figure 2d,e).

These results showed that the NO-cGMP-cGKI signalling axis is functionally expressed in HSCs of the mouse livers. Importantly, cell type-specific knockout of cGKI in HSCs resulted in increased HSC activation in aged animals, suggesting that disruption of the NO-cGMP signalling cascade could elevate the risk of liver disease.

3.3 | Expression of NO-GC and cGKI is maintained in hepatic stellate cells (HSCs) of metabolic dysfunction-associated steatohepatitis (MASH) livers

After observing evidence that the NO-cGMP-cGKI signalling axis is expressed in activated HSCs in vitro (Figure 1) and that its genetic inhibition results in pathological changes in aged HSC-cGKI-KO mice, we investigated the relevance of the cGMP signalling pathway in the context of chronic liver disease. HSC activation contributes to MASH, which is often associated with diabetes and cardiovascular diseases (Wojcik-Cichy et al., 2018). We used ApoE KO mice on an HFD, an established mouse model to study human MASH (Camargo et al., 2022; Schierwagen et al., 2015) and atherosclerosis (Zhang et al., 1992). We modified this model by extending the feeding time from 7 to 18 weeks in order to induce advanced atherosclerosis in the animals. We then analysed MASH in both sexes. Ten-week-old homozygous ApoE KO mice were fed a HFD for 18 weeks (hereafter referred to as MASH mice). Heterozygous litter-matched ApoE KO mice fed a normal diet served as controls (hereafter referred to as control mice).

Compared with control mice, male and female MASH mice showed a significant increase in body weight (Figure 3a) and liver-to-body weight ratio (Figure 3b), indicating steatosis and hepatomegaly. Next, we analysed the expression and localization of NO-GC and cGKI in MASH livers. Western blot analysis revealed a marked increase in NO-GC and cGKI expression in MASH livers of both male and female mice compared with healthy control livers, accompanied by elevated levels of the HSC activation marker SM22α in MASH livers (Figure 3c). As no significant differences were detected between control males and females or MASH males and females, both sexes were pooled for quantitative analysis

FIGURE 3 Analysis of NO-GC and cGKI expression in healthy and metabolic dysfunction-associated steatohepatitis (MASH) livers. (a) Body weight and (b) liver-to-body weight (LW/BW) ratio of male mice (ctrl: $n = 5$, MASH: $n = 8$) and female mice (ctrl: $n = 5$, MASH: $n = 11$). (c) Western blot analysis of SM22α, NO-GC and cGKI expression in livers from male (ctrl: $n = 3$, MASH: $n = 3$) and female mice (ctrl: $n = 3$, MASH: $n = 3$) and (d) the corresponding quantification of data from (c) with males and females pooled. Data are represented as mean ± SEM. *P*-values obtained with the Mann–Whitney *U*-test are indicated. (e–h) Immunofluorescence staining of liver sections from control mice (left images) and MASH mice (right images) for (e) SM22α (green), (f) NO-GC (green) and (g) cGKI (green). Representative images from male mice (3 sections from 3 ctrl and 3 sections from 3 MASH mice) show (from left to right) an overview picture and a magnified overlay image of the framed region with arrows denoting hepatic stellate cells (HSCs) and arrowheads denoting non-HSCs. Nuclei are shown in blue. (h) Immunofluorescence co-staining of the HSC marker desmin (green) with NO-GC (red, left panels) or cGKI (red, right panels) and nuclei (blue) on liver sections from MASH mice. Representative images from male mice (3 sections from 3 MASH mice) show (from left to right) staining of desmin and a magnified overlay image. The arrows indicate co-localization of desmin with NO-GC or cGKI in HSCs. Scale bars, 50 μm. Ctrl, control.

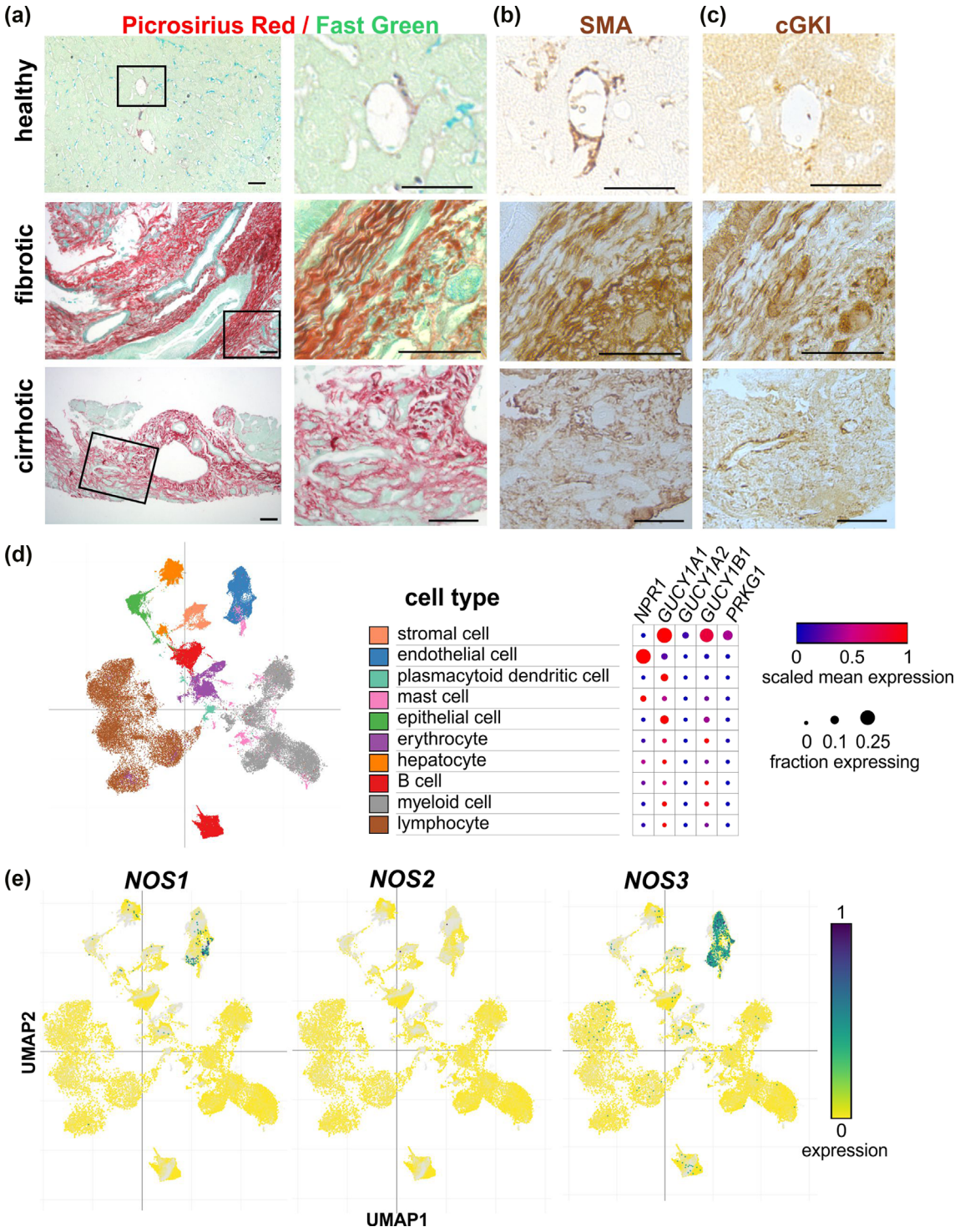

FIGURE 4 Expression of components of the cGMP-axis in the human liver. (a–c) Sections of healthy (up), fibrotic (middle) and cirrhotic (low) human livers stained with (a) picrosirius red and fast green to visualize collagen fibres (red). Magnification of the boxed region (a, right). (b, c) Immunostaining of α-smooth muscle actin (SMA) (b, brown) and cGKI (c, brown) in serial sections corresponding to the respective sections in (a). Scale bars, 50 μm. (d–e) Analyses of publicly available scRNA-seq data (Fabre et al., 2023) from human liver for the expression of genes involved in the cGMP signalling pathway. (d) UMAP visualization of cell clusters and their identification (left), and expression of the cGMP pathway genes *NPR1*, *GUCY1A1*, *GUCY1A2*, *GUCY1B1* and *PRKG1* in the identified clusters (right). The colour scale indicates the expression level normalized across all clusters (blue, low; red, high). The size of each dot shows the percentage of cells per cluster with at least one detected transcript for the respective gene. (e) UMAP visualization of *NOS1*, *NOS2* and *NOS3* mRNA expression in all liver cells. The colour scale indicates expression levels (yellow, low; blue, high).

TABLE 1 Analysis of body weight, blood pressure and livers from metabolic dysfunction-associated steatohepatitis (MASH) and MASH + NO-GC activator BAY-543 (Act) mice at the end of the experiment.

	Males		Females	
	MASH	MASH + Act	MASH	MASH + Act
	($n = 7$)	($n = 8$)	($n = 8$)	($n = 8$)
Body weight (g)	34.5 ± 1.6	30.6 ± 1.0	31.7 ± 0.8	29.8 ± 1.3
	($n = 6$)	($n = 6$)	($n = 4$)	($n = 4$)
Systolic blood pressure (mmHg)	107.2 ± 8.0	109.9 ± 7.0	103.7 ± 7.6	111.9 ± 11.1
Diastolic blood pressure (mmHg)	76.6 ± 7.5	74.6 ± 5.1	74.6 ± 7.2	81.3 ± 9.7
	($n = 7$)	($n = 5$)	($n = 7$)	($n = 5$)
Macro-steatosis score (%)	47 ± 8	18 ± 3*	14 ± 1	7 ± 2*
Fibrosis score (Ishak score)	1.4 ± 0.2	0.6 ± 0.2	2.4 ± 0.4	0.2 ± 0.1**
	($n = 8$)	($n = 7$)	($n = 12$)	($n = 8$)
Liver triglycerides (mg/100 mg tissue)	19.9 ± 6.6	13.3 ± 3.1*	16.0 ± 6.3	14.3 ± 4.3
Liver cholesterol (mg/100 mg tissue)	2.6 ± 1.2	1.6 ± 0.6	2.5 ± 1.0	2.0 ± 0.8

Note: Data are shown as mean ± SEM. Statistical significance of MASH + Act male versus MASH male or MASH + Act female versus MASH female mice is indicated by asterisks (*$P < 0.05$, **$P < 0.01$). *P*-values were obtained with the Mann–Whitney *U*-test.

(Figure 3d). An enrichment of SM22α-positive cells in MASH livers versus controls was also detected via immunofluorescence staining (Figure 3e), indicating that HSCs were activated in our MASH model. As expected from previous studies (Lutz et al., 2011; Theilig et al., 2001), immunofluorescence staining of liver sections of healthy controls revealed NO-GC- and cGKI-positive cells with a morphology characteristic for the quiescent HSC phenotype (Figure 3f,g, white arrows in left panels). Consistent with our analysis of primary HSC cultures, MASH livers displayed clusters of NO-GC- and cGKI-positive presumably activated HSCs (Figure 3f,g, white arrows in right panels). Co-staining with the murine HSC marker desmin confirmed that the NO-GC- and cGKI-expressing cells in our MASH model were HSCs (Figure 3h, white arrows). Additionally, the percentage of desmin-positive cells in MASH livers was significantly higher than in controls (MASH 35% ± 9% versus control 16% ± 2% of total cells, $n = 3$ sections from 3 male mice each). Similarly, and in agreement with our Western blot data (Figure 3c,d), the fraction of NO-GC-positive HSCs (Figure 3f, MASH 27% ± 9% versus controls 13% ± 1% of total cells, $n = 3$ sections from 3 male mice each) and cGKI-expressing HSCs (Figure 3g, MASH 30% ± 3% versus controls 6% ± 1% of total cells, $n = 3$ sections from 3 male mice each) increased strongly in MASH livers compared with controls. NO-GC and cGKI expression were also observed in smooth muscle cells of the hepatic vasculature (data not shown), whereas liver cells with larger nuclei, presumably mainly hepatocytes, did not stain positive for NO-GC or cGKI (Figure 3f–g, white arrowheads). The latter results were consistent with earlier studies in which these proteins were also not detected in hepatocytes or other non-HSCs except vascular smooth muscle cells (Lutz et al., 2011; Theilig et al., 2001).

Together, our findings suggested that ApoE KO mice on an HFD are an appropriate model for analysing cGMP signalling in MASH, where high NO-GC and cGKI expression was mainly due to the increased number of activated HSCs arranged in clusters. Interestingly, we found that NO-GC and cGKI are expressed in HSCs in both healthy and MASH livers and could be explored as potential targets for novel treatment strategies of MASH.

3.4 | cGKI is strongly expressed in fibrotic and cirrhotic human livers

To investigate whether our findings in mice might also translate to humans, we analysed liver sections from humans with a healthy liver and patients diagnosed as having hepatic fibrosis or cirrhosis (Figure 4). Staining with picrosirius red and fast green confirmed extensive fibrosis in fibrotic and cirrhotic liver samples, indicated by red-stained perivascular fibres and bridges, which were only weakly detectable in healthy liver tissue (Figure 4a). Serial sections of regions that were strongly stained red by picrosirius red also showed strong SMA expression, indicating activated HSCs in these fibrotic areas (Figure 4b). Consistent with our findings in murine livers, cGKI expression was strongly elevated in fibrotic and cirrhotic human livers as compared with healthy liver samples (Figure 4c). In addition to immunostaining of liver sections, we re-analysed publicly available scRNA-seq datasets from human liver for the expression of genes involved in the cGMP signalling pathway (Fabre et al., 2023). We found that the mRNAs for *GUCY1A1* and *GUCY1B1* (encoding the α1 and β1 subunit of NO-GC, respectively), as well as the mRNA for the cGMP effector *PRKG1* (encoding cGKI), were strongly expressed in stromal cells containing HSCs/myofibroblasts, whereas these mRNAs were barely detectable in other liver cell types (Figure 4d). In contrast, mRNAs for the membrane-associated *NPR1* (encoding GC-A, the receptor for atrial natriuretic peptide) and the NO generator *NOS3* (encoding eNOS) were preferentially expressed in endothelial cells (Figure 4d,e). Other NO generators like *NOS1* (encoding nNOS) and *NOS2* (encoding iNOS) were detected only in a few endothelial cells or not at all (Figure 4e). The mRNA expression profile of the analysed genes was similar in healthy and diseased livers (data not shown).

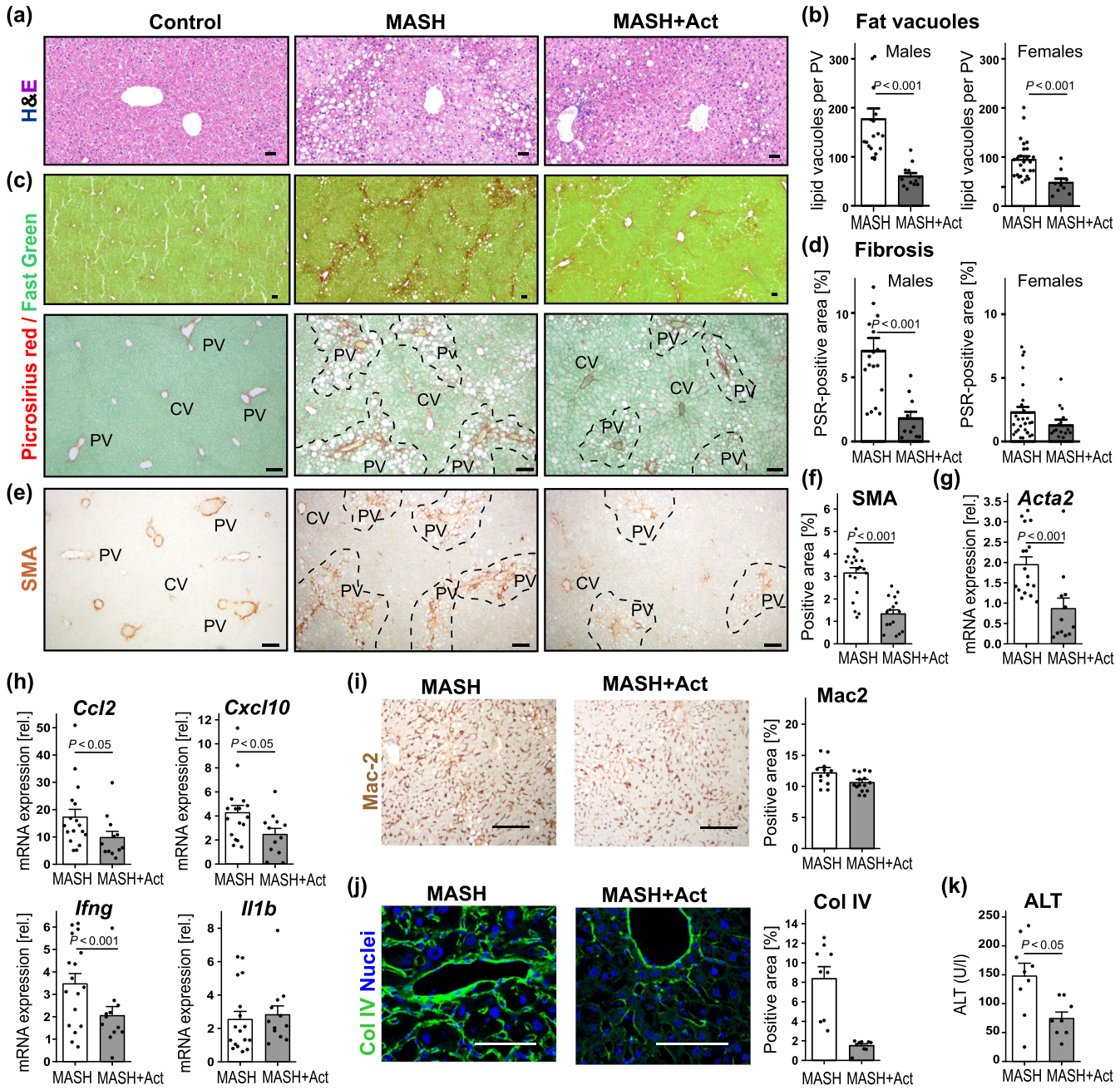

FIGURE 5 Characterization of metabolic dysfunction-associated steatohepatitis (MASH) livers from mice treated with the NO-GC activator BAY-543 (Act). (a, c, e) Representative images of liver sections from control (left), MASH (middle) and MASH + Act (right) mice. (a) Haematoxylin and eosin staining and (b) lipid vacuole count per portal vein in MASH (18 sections from 6 males, 27 sections from 9 females) and MASH + Act (12 sections from 4 males, 9 sections from 3 females) livers. (c) Picrosirius red and fast green staining. Higher magnification is shown in the lower panels. (d) Quantification of the picrosirius red-positive area in MASH (18 sections from 6 males, 26 sections from 9 females) and MASH + Act (10 sections from 4 males; 15 sections from 6 females) livers. Note that the MASH male group contained one data point above 450 in (b) and above 19 in (d). These data points are not shown in the bar graphs but are included in the statistical analysis. (e) Immunohistochemistry staining of SMA. (f–k) Since there were no significant differences between males and females, the data were pooled for quantification. (f) Quantification of the α-smooth muscle actin (SMA)-positive area in MASH (20 sections from 5 mice) and MASH + Act (16 sections from 4 mice) livers. (g–h) Transcript levels of (g) Acta2, (h) Ccl2, Cxcl10, Ifng and Il1b in the livers of MASH ($n = 17$) and MASH + Act ($n = 12$) mice were quantified by RT-PCR and normalized to wild-type animals on normal diet. (i) Immunohistochemistry staining of Mac-2 and quantification of the Mac-2-positive area in MASH (12 sections from 4 mice) and MASH + Act (15 sections from 5 mice) livers. (j) Immunofluorescence staining of collagen IV and quantification of the collagen IV-positive area in MASH (9 sections from 3 mice) and MASH + Act (9 sections from 3 mice) livers. (k) Serum levels of alanine aminotransferase (ALT) in MASH ($n = 9$) and MASH + Act ($n = 8$) mice. Data are represented as mean ± SEM. Where n=3 or 4 independent experiments (i, j), statistical analysis was not carried out, and results should be regarded as preliminary. *P*-values were obtained with the Mann–Whitney *U*-test. Scale bars, 50 μm. CV, central vein; PV, portal vein; dashed lines indicate the steatotic and fibrotic regions around the PV.

Together, these findings suggested that fibrotic regions in human liver contain extracellular matrix-producing activated HSCs, which express NO-GC and cGKI, whereas the main source of NO is endothelial cells expressing eNOS.

3.5 | The NO-GC activator BAY-543 improves metabolic dysfunction-associated steatohepatitis (MASH)

To evaluate the therapeutic potential of targeting the NO-cGMP axis in HSCs in MASH, we stimulated the signalling pathway by treating MASH mice with the NO-GC activator BAY-543 (Act), which increased the cGMP concentration in activated HSCs (Figure 1l,m). We hypothesized that BAY-543 could be efficient under oxidative stress conditions that might occur in MASH, enabling activation of oxidized forms of NO-GC that do not respond adequately to NO or NO-GC stimulators (Dai & Stuehr, 2025; Sandner et al., 2021). To test if activation of NO-GC with BAY-543 improves MASH, we compared healthy control mice, MASH mice and MASH mice fed a HFD supplemented with BAY-543 (hereafter referred to as MASH + Act mice). Treatment with BAY-543 resulted in a concentration of 16.6 ± 2 nM ($n = 8$ animals) of the unbound fraction of BAY-543 in the plasma of MASH + Act animals. Considering the concentrations of BAY-543 (1 nm or 10 nM) that induce cGMP in cultured HSCs (Figure 1l,m), this plasma concentration is within a sufficient range to enhance cGMP in HSCs in the liver in vivo. Importantly, this concentration of BAY-543 did not significantly change blood pressure in male and female animals (Table 1).

MASH and MASH + Act mice displayed prominent hepatic fat accumulation in comparison to control mice, evident as both macro- and micro-steatosis (Figure 5a). Micro-steatosis was consistently observed around the central veins, whereas macro-steatosis was found in a subcapsular pattern and showed a portal-to-portal distribution. The overall pattern of fat distribution was similar in MASH mice and MASH + Act mice, with no evidence of ballooning or necrosis observed. However, macro-steatosis, analysed by a pathologist, was significantly reduced by ≈50% in livers from MASH + Act versus MASH animals, with the males in the MASH group showing higher variation than all other groups (Table 1). We confirmed the decrease in macro-steatosis by quantitative analysis of lipid vacuole buildup around the portal vein of liver sections, which was significantly reduced in both sexes (Figure 5b). Triglyceride and cholesterol levels in liver tissue showed a trend towards lower values in male and female MASH + Act mice compared with MASH animals (Table 1). Portal-to-portal fibrosis was less pronounced in MASH + Act versus MASH livers (Figure 5c). The quantitative assessment of fibrosis using picrosirius red staining (Figure 5d) and the Ishak fibrosis score (Table 1) showed a reduction in fibrosis in both males and females. However, statistical significance was not reached for the Ishak fibrosis score in males (Table 1) and for picrosirius red data in females (Figure 5d).

To test if steatosis and fibrosis were associated with elevated expression of the HSC activation marker SMA, we stained liver sections with an SMA-specific antibody. Indeed, the SMA-positive area was strongly increased in MASH mice compared with healthy controls (Figure 5e). To obtain a higher animal number for further analysis, the two sexes were compared with each other. Since no significant differences were found between males and females in the MASH or MASH + Act groups, both sexes were pooled. The increase in the SMA-positive area was significantly reduced in MASH + Act animals (Figure 5f). Consistent with the protein changes seen in tissue sections, a similar reduction was observed at the level of *Acta2* mRNA (encoding SMA) in the MASH + Act group versus MASH mice (Figure 5g). The similar distribution of macro-steatosis and fibrosis in the portal-to-portal region (Figure 5c) suggested that reduced HSC activation and fibrosis in the MASH + Act group could also affect fat distribution in the liver.

Furthermore, markers of liver inflammation were decreased in the MASH + Act mice compared with the MASH group. Transcript levels of the chemokines *Ccl2* and *Cxcl10*, and of the cytokine *Ifng*, but not *Il1b*, were significantly reduced in MASH + Act versus MASH livers (Figure 5h). Immunostaining demonstrated a lower number of Mac-2-positive macrophages (Figure 5i) and a dramatically decreased collagen IV content (Figure 5j) in MASH + Act versus MASH livers. In addition, plasma level of alanine aminotransferase, a marker of liver injury, was significantly lower in MASH + Act than MASH mice (Figure 5k), indicating less liver damage in mice treated with the NO-GC activator.

Together, these results demonstrated that the ApoE KO/HFD MASH mouse model is suitable for the investigation of steatosis, fibrosis and liver inflammation in both male and female mice. Importantly, treatment of MASH mice with the NO-GC activator BAY-543 significantly improved multiple features of MASH progression.

4 | DISCUSSION AND CONCLUSIONS

The chronic liver disease MASH is primarily caused by overnutrition and a sedentary lifestyle and can lead to severe complications in its advanced stages (Hagstrom et al., 2024). Numerous drugs have been developed to inhibit MASH, targeting different cell types or signalling pathways. The approaches have not yet led to the desired improvement in clinical outcomes and are often associated with side effects that lead to discontinuation of therapy (Zhao et al., 2022). During MASH progression, HSCs are activated, proliferate and transform into fibrogenic myofibroblasts (Kisseleva & Brenner, 2021; Tsuchida & Friedman, 2017). In the present study, we found that the NO-NO-GC-cGMP-cGKI signalling axis is expressed in both quiescent and activated HSCs and that pharmacological stimulation of this pathway with the NO-GC activator BAY-543 might present a new treatment option for MASH.

In the healthy liver, HSCs remain in a quiescent state characterized by vitamin A metabolism and storage within cytoplasmic lipid droplets. Persistent liver injury causes the activation of HSCs and their transdifferentiation into collagen-producing, pro-inflammatory HSCs/myofibroblasts (Kisseleva & Brenner, 2021; Tsuchida & Friedman, 2017). We observed that primary murine HSCs cultured for

8 days developed a myofibroblast phenotype like activated HSCs during liver fibrosis, which is consistent with the results reported by Dang et al. (2021). The activated HSCs expressed key cGMP signalling proteins, specifically the cGMP generator NO-GC and the cGMP downstream effector cGKI. The functionality of NO-cGMP signalling in HSCs was analysed by live-cell imaging of HSCs expressing a cGMP indicator protein. This technique allowed us to monitor cGMP signals in HSCs in real time with spatiotemporal resolution. The NO donor DEA-NO triggered cGMP elevations in both quiescent and activated HSCs. Interestingly, NO-induced cGMP signals were weaker when HSCs were more activated (Figure 1k, Day 8 vs. Day 2). In contrast, cGMP increases stimulated by the pharmacological NO-GC activator BAY-543 were not attenuated in activated HSCs (Figure 1l,m, Day 8 vs. Day 2). These findings suggest that the NO-cGMP signalling pathway is expressed in activated HSCs, but its functionality is limited, possibly because NO-GC is partially oxidized in activated HSCs, resulting in reduced sensitivity to NO. However, BAY-543 could circumvent this limitation by acting on the oxidized NO-GC (Dai & Stuehr, 2025; Sandner et al., 2021).

To study NO-cGMP signalling in HSCs located in their natural environment in the liver, we used whole liver preparations of HSC-specific cGMP sensor mice. In these liver preparations, NO-induced cGMP signals were detected in HSCs, suggesting the presence of a functional NO-cGMP signalling pathway in HSCs in vivo. Importantly, genetic ablation of the cGMP effector cGKI specifically in HSCs led to increased HSC activation in aged knockout mice. Activation of HSCs induced by the reduction of cGKI has so far only been demonstrated in HSCs in vitro (Franko et al., 2018). These results, together with the previous finding that genetic ablation of cGKI in non-smooth muscle cells, including HSCs, resulted in a complex metabolic phenotype with liver inflammation and fasting hyperglycaemia (Lutz et al., 2011), provide evidence that impaired NO-cGMP-cGKI signalling in HSCs leads to increased HSC activation.

In the Western world, MASLD and its more advanced stage, MASH, are typically accompanied by obesity (Friedman et al., 2018). Additionally, phenotypic profiling of patient material showed at least two distinct types of MASLD, one associated with limited risk and one associated with higher risk of cardiovascular diseases (Jamialahmadi et al., 2024; Raverdy et al., 2024). Therefore, from the multitude of rodent MASLD/MASH models (Schonke & Rensen, 2024), we chose a model that reflects the situation in patients with hepatic steatosis and an increased risk of cardiovascular disease. The ApoE KO mouse model combines characteristic features of atherosclerosis (Zhang et al., 1992) and MASH (Camargo et al., 2022; Schierwagen et al., 2015). In comparison with previous MASH studies with ApoE KO mice, we extended HFD feeding from 7 to 18 weeks to prolong the time for the development of liver fibrosis. Similar to the published data for male mice, we observed key features of MASH in male and female mice, including (i) weight gain and hepatomegaly, (ii) hepatic steatosis and (iii) HSC activation associated with fibrosis and inflammation. Some effects in this model, such as liver to body weight ratio or steatosis, were more pronounced in males but with a higher variability in comparison to female animals. In addition to the up-regulation of the HSC activation markers SMA and SM22α, we also detected increased expression of components of the NO-cGMP pathway in MASH livers, namely, NO-GC and cGKI. However, NO-GC and cGKI were expressed not only in activated HSCs but also in quiescent HSCs in healthy livers, similar to the HSC marker desmin.

Expression of NO-GC and cGKI in HSCs was recently reported in scRNA-seq studies in both human and mouse livers (He et al., 2023; Yang et al., 2021). scRNA-seq studies have also shown that there is marked heterogeneity among HSC subpopulations in mouse and human livers, as recently summarized by Geng and Schwabe (Geng & Schwabe, 2025). The different HSC subpopulations may play opposing roles in promoting or inhibiting liver fibrosis and carcinogenesis (Filliol et al., 2022). Although we were able to detect functional NO-cGMP signalling in both quiescent and activated HSCs, the exact expression profile of NO-GC and cGKI and their functional relevance in the various HSC subpopulations has not yet been clarified.

He et al. characterized HSC signatures in healthy and MASH-affected human livers, showing that *GUCY1A1* and *GUCY1B1* mRNA (encoding the α_1 and β_1 subunits of NO-GC, respectively), as well as *PRKG1* mRNA (encoding cGKI), are among the most highly expressed genes in resting HSCs of healthy livers (He et al., 2023). Using carbon tetrachloride and bile duct ligation fibrosis models, Yang et al. (2021) reported differential gene expression between portal fibroblasts and HSCs, with NO-GC exclusively expressed in HSCs but absent in portal fibroblasts. The authors grouped HSCs into four clusters representing quiescent HSCs and three stages of activated HSCs. The mRNA expression levels of the NO-GC subunits *Gucy1a1* and *Gucy1b1* per cell decreased following HSC activation, reaching their lowest levels in Stage 3 activated HSCs. By contrast, increased protein expression of NO-GC and cGKI was detected in whole liver tissues of different mouse and rat fibrosis models without analysis at cellular resolution (Sorz-Nechay et al., 2025). We showed the expression of NO-GC and cGKI in HSCs, detected at the protein level with highly specific antibodies against the β1 subunit of NO-GC or cGKI and, more importantly, the functional activity of the NO-cGMP signalling pathway in HSCs, demonstrated by live-cell imaging. In the MASH livers of our ApoE KO model, NO-GC and cGKI were up-regulated and expressed in activated HSCs that had accumulated in clusters in the fibrotic livers. Moreover, we show that NO-GC and cGKI were expressed in HSCs of diseased human liver. The cGKI-positive cells are localized particularly in fibrotic areas, where SMA, a marker for activated HSCs, is also significantly elevated. Together, the previous reports (Sorz-Nechay et al., 2025) and our present data indicate that the NO-cGMP-cGKI axis is selectively expressed in quiescent and activated HSCs in mice and humans and could serve as a drug target in MASH.

Equally important as expression is the functionality of the signalling pathway. It is interesting to note that cGKI in HSCs could also be activated independently of NO-GC by cGMP from alternative sources, such as atrial natriuretic peptide- or C-type natriuretic peptide-induced guanylyl cyclases (Perez-Ternero et al., 2025; Suzuki et al., 2023; Tao et al., 1999). The heterogeneous cGMP signalling (Feil et al., 2022) within HSCs at different activation stages and

between HSCs and other cell types, such as portal fibroblasts, may play a diverse role in the pathology of MASH.

Reduced NO-induced cGMP signals in the activated HSCs expressing NO-GC indicated that oxidative stress conditions in MASH might cause not only HSC activation (Tsuchida & Friedman, 2017) but also oxidation of the NO-binding haem group of NO-GC, rendering the enzyme unresponsive to NO (Stasch et al., 2015). Unlike NO-GC stimulators, NO-GC activators target and activate forms of NO-GC that are insensitive to NO (Dai & Stuehr, 2025). Therefore, NO-GC activators may be advantageous compared with NO-GC stimulators in chronic conditions, such as MASH, that are associated with increased oxidative stress. Our cGMP imaging data in primary HSCs are consistent with this assumption. Even though NO-GC and cGKI were clearly expressed in the activated HSCs, the cGMP increase, which could be induced by NO, was attenuated compared to the BAY-543-induced cGMP increase.

Published studies on NO-GC activators other than BAY-543 have been conducted in severe fibrosis models without steatosis, only in male rats, and are not yet conclusive. One of the first NO-GC activators, **Cinaciguat**, was compared with the NO-GC stimulator **Riociguat** in the bile duct ligation model. Cinaciguat did not show improvement in liver fibrosis, but caused arterial hypotension, whereas Riociguat significantly decreased fibrosis without effects on the mean arterial blood pressure (Brusilovskaya et al., 2020). Other NO-GC activators showed a dose-dependent reduction of fibrosis in carbon tetrachloride- or pig serum-induced liver fibrosis (Knorr et al., 2008) or in a thioacetamide-induced cirrhosis model (Jones et al., 2023), with higher doses affecting blood pressure. These results indicated that the effects of NO-GC stimulators or activators on fibrosis should be evaluated depending on the dosing, which can influence extrahepatic effects or blood pressure. In a rat model for renal fibrosis, the direct comparison of an NO-GC stimulator and an NO-GC activator showed comparable blood pressure–lowering effects, but fibrosis was only reduced with the activator BAY 60–2770 (X. Chen et al., 2024).

In our mouse MASH model, chronic treatment with the NO-GC activator BAY-543 added to the diet led to plasma concentrations of unbound BAY-543 that could effectively induce cGMP elevation in activated HSCs in culture. The treatment did not result in changes of blood pressure, but it did reduce macro-steatosis, fibrosis, inflammation and the expression of indicators of activated HSCs in both male and female mice, as compared with the untreated MASH group.

Our findings suggest that activation of the NO-cGMP axis in HSCs suppresses the transition of quiescent HSCs into activated HSCs and/or the proliferation of activated HSCs, resulting in notable antifibrotic effects associated with less steatosis and hepatic inflammation. The endogenous mechanism underlying these effects is likely initiated by the diffusion of NO from endothelial cells into HSCs. There, NO-GC, cGMP generation and cGKI are activated, which could then affect the phenotype and growth of the HSCs. A similar mechanism has been previously described for the NO-cGMP-dependent regulation of vascular smooth muscle cells (Weinmeister et al., 2008; Wolfsgruber et al., 2003). cGKI could also inhibit migration/chemotaxis or the formation of focal adhesions in HSCs as suggested by Routray et al. (2011). In MASH, oxidative stress could increase the level of oxidized NO-GC that no longer responds to NO but can be activated by BAY-543. BAY-543 not only improved liver function, as evidenced by reduced alanine aminotransferase levels, but also led to antifibrotic effects associated with reduced hepatic inflammation and macro-steatosis. A recent study by Feng et al. (2025) showed that a novel **PDE5** inhibitor exerts similar therapeutic effects on liver fibrosis as BAY-543 via the NO-cGMP-cGKI axis and the suppression of key pro-fibrotic pathways, including **TGFβ**/Smad and **Akt**/**NF-κB** signalling. However, we cannot fully exclude cGMP-independent effects of BAY-543, as has been reported for an NO-GC stimulator (P. J. Chen et al., 2020). In addition, NO as well as BAY-543 could have effects on non-HSCs in and outside the liver. For instance, the reduction of macro-steatosis observed after BAY-543 treatment could be independent of its antifibrotic effects in HSCs. Indeed, genetic ablation of cGKI in mice showed a complex metabolic phenotype indicating a positive effect of cGMP signalling on liver health (Lutz et al., 2011). Therefore, the improvements in steatosis and alanine aminotransferase levels could be attributed not only to the specific effects of BAY-543 on HSCs but also to systemic or non-HSC-mediated effects of the drug.

In this study, we analysed cGMP signalling in primary HSCs and whole liver tissue via live-cell imaging in combination with newly developed HSC-specific mouse models, chose a MASH mouse model reflecting the situation in humans with comorbidities and compared male and female animals. We could show that the NO-cGMP-cGKI signalling axis is patho-physiologically important in activated HSCs of MASH mice and that it is also relevant for patients with liver diseases. The NO-GC activator BAY-543 studied in our mouse model effectively reduced features of MASH. Overall, the maintenance of cGMP signalling by BAY-543 could make an important contribution to controlling the function of HSCs and thus represent a new therapeutic option for the treatment of MASH in humans.

AUTHOR CONTRIBUTIONS

Krithika Rajeeth: Writing—original draft; methodology; data curation; validation; investigation; formal analysis; visualization; writing—review and editing. **Malte Roessing:** Methodology; investigation; resources. **Moritz Lehners:** Methodology; software; validation; formal analysis; visualization. **Lisa Dietz:** Methodology; data curation. **Anja Schmitt:** Methodology; data curation. **Stephan Hailfinger:** Methodology. **Andreas Peter:** Methodology; data curation. **Leticia Quinanilla-Martinez:** Methodology; data curation. **Irene Gonzalez-Menendez:** Methodology; data curation. **Ingmar Mederacke:** Methodology. **German Ott:** Methodology; data curation. **Peter Sandner:** Methodology; formal analysis; validation; data curation. **Matthias Schwab:** Methodology; data curation; validation. **Robert Feil:** Methodology; data curation; writing—review and editing; funding acquisition; validation; conceptualization; supervision. **Susanne Feil:** Methodology; data curation; investigation; formal analysis; project administration; writing—review and editing; funding acquisition; supervision; visualization; validation; conceptualization.

ACKNOWLEDGEMENTS

We thank Barbara Birk for technical assistance. Special thanks go to all members of the Feil laboratory including lab students, specifically Miriam Rupprecht, for experimental support and constructive discussions as well as to the staff of the animal facility. Open Access funding enabled and organized by Projekt DEAL.

CONFLICT OF INTEREST STATEMENT

The authors declare no conflicts of interest.

DATA AVAILABILITY STATEMENT

The data that support the findings of this study are available from the corresponding author upon reasonable request.

DECLARATION OF TRANSPARENCY AND SCIENTIFIC RIGOUR

This declaration acknowledges that this paper adheres to the principles for transparent reporting and scientific rigour of preclinical research as stated in the BJP guidelines for Natural Products Research, Design and Analysis, Immunoblotting and Immunochemistry and Animal Experimentation and as recommended by funding agencies, publishers and other organizations engaged with supporting research.

ORCID

Peter Sandner https://orcid.org/0000-0003-2977-7553
Robert Feil https://orcid.org/0000-0002-7335-4841
Susanne Feil https://orcid.org/0000-0003-2148-8773

REFERENCES

Alexander, S. P. H., Fabbro, D., Gibb, A. J., Kelly, E., Mathie, A. A., Peach, C. J., Veale, E. L., Armstrong, J. F., Faccenda, E., Harding, S. D., Southan, C., Davies, J. A., Annett, S., Boison, D., Burns, K. E., Dessauer, C., Gertsch, J., Helsby, N. A., Izzo, A. A., … Wong, S. S. (2025). The Concise Guide to PHARMACOLOGY 2025/26: Enzymes. *British Journal of Pharmacology*, *182*(Suppl 1), S307–S403. https://doi.org/10.1111/bph.70234

Alexander, S. P. H., Fabbro, D., Peach, C. J., Gibb, A. J., Kelly, E., Mathie, A. A., Veale, E. L., Armstrong, J. F., Faccenda, E., Harding, S. D., Southan, C., Davies, J. A., Beuve, A., Brouckaert, P., Bryant, C., Burnett, J. C., Farndale, R. W., Friebe, A., Garthwaite, J., … Waldman, S. A. (2025). The Concise Guide to PHARMACOLOGY 2025/26: Catalytic receptors. *British Journal of Pharmacology*, *182*-(Suppl 1), S259–S306. https://doi.org/10.1111/bph.70233

Alexander, S. P. H., Gibb, A. J., Kelly, E., Mathie, A. A., Peach, C. J., Veale, E. L., Cidlowski, J. A., Davenport, A. P., Fabbro, D., Spedding, M., Striessnig, J., Armstrong, J. F., Buneman, O. P., Faccenda, E., Harding, S. D., Southan, C., Davies, J. A., Ahlers-Dannen, K. E., Alqinyah, M., … Zolghadri, Y. (2025). The Concise Guide to PHARMACOLOGY 2025/26: Introduction and Other Protein Targets. *British Journal of Pharmacology*, *182*(Suppl 1), S1–S23. https://doi.org/10.1111/bph.70229

Alexander, S. P. H., Roberts, R. E., Broughton, B. R. S., Sobey, C. G., George, C. H., Stanford, S. C., Cirino, G., Docherty, J. R., Giembycz, M. A., Hoyer, D., Insel, P. A., Izzo, A. A., Ji, Y., MacEwan, D. J., Mangum, J., Wonnacott, S., & Ahluwalia, A. (2018). Goals and practicalities of immunoblotting and immunohistochemistry: A guide for submission to the British Journal of Pharmacology. *British Journal of Pharmacology*, *175*, 407–411. https://doi.org/10.1111/bph.14112

Anstee, Q. M., Reeves, H. L., Kotsiliti, E., Govaere, O., & Heikenwalder, M. (2019). From NASH to HCC: Current concepts and future challenges. *Nature Reviews. Gastroenterology & Hepatology*, *16*(7), 411–428. https://doi.org/10.1038/s41575-019-0145-7

Bankhead, P., Loughrey, M. B., Fernandez, J. A., Dombrowski, Y., McArt, D. G., Dunne, P. D., McQuaid, S., Gray, R. T., Murray, L. J., Coleman, H. G., James, J. A., Salto-Tellez, M., & Hamilton, P. W. (2017). QuPath: Open source software for digital pathology image analysis. *Scientific Reports*, *7*(1), 16878. https://doi.org/10.1038/s41598-017-17204-5

Beavo, J. A., & Brunton, L. L. (2002). Cyclic nucleotide research—Still expanding after half a century. *Nature Reviews. Molecular Cell Biology*, *3*(9), 710–718. https://doi.org/10.1038/nrm911

Bender, A. T., & Beavo, J. A. (2006). Cyclic nucleotide phosphodiesterases: Molecular regulation to clinical use. *Pharmacological Reviews*, *58*(3), 488–520. https://doi.org/10.1124/pr.58.3.5

Brusilovskaya, K., Konigshofer, P., Lampach, D., Szodl, A., Supper, P., Bauer, D., Beer, A., Stift, J., Timelthaler, G., Oberhuber, G., Podesser, B. K., Seif, M., Zinober, K., Rohr-Udilova, N., Trauner, M., Reiberger, T., & Schwabl, P. (2020). Soluble guanylyl cyclase stimulation and phosphodiesterase-5 inhibition improve portal hypertension and reduce liver fibrosis in bile duct-ligated rats. *United European Gastroenterology Journal*, *8*(10), 1174–1185. https://doi.org/10.1177/2050640620944140

Camargo, F. N., Matos, S. L., Araujo, L. C. C., Carvalho, C. R. O., Amaral, A. G., & Camporez, J. P. (2022). Western diet-fed ApoE knockout male mice as an experimental model of non-alcoholic steatohepatitis. *Current Issues in Molecular Biology*, *44*(10), 4692–4703. https://doi.org/10.3390/cimb44100320

Chen, P. J., Kuo, L. M., Wu, Y. H., Chang, Y. C., Lai, K. H., & Hwang, T. L. (2020). BAY 41-2272 attenuates CTGF expression via sGC/cGMP-independent pathway in TGFbeta1-activated hepatic stellate cells. *Biomedicine*, *8*(9), 330. https://doi.org/10.3390/biomedicines8090330

Chen, X., Xiong, Y., Zeng, S., Delić, D., Gaballa, M., Kalk, P., … Hocher, B. (2024). Comparison of sGC activator and sGC stimulator in 5/6 nephrectomized rats on high-salt-diet. *Frontiers in Pharmacology*, *15*, 1480186. https://doi.org/10.3389/fphar.2024.1480186

Curtis, M. J., Alexander, S. P. H., Cortese-Krott, M., Kendall, D. A., Martemyanov, K. A., Mauro, C., Panettieri, R. A. Jr., Papapetropoulos, A., Patel, H. H., Santo, E. E., Schulz, R., Stefanska, B., Stephens, G. J., Teixeira, M. M., Vergnolle, N., Wang, X., & Ferdinandy, P. (2025). Guidance on the planning and reporting of experimental design and analysis. *British Journal of Pharmacology*, *182*(7), 1413–1415. https://doi.org/10.1111/bph.17441

Dai, Y., & Stuehr, D. J. (2025). Heme delivery into soluble guanylyl cyclase requires a heme redox change and is regulated by NO and Hsp90 by distinct mechanisms. *The Journal of Biological Chemistry*, *301*(3), 108315. https://doi.org/10.1016/j.jbc.2025.108315

Dang, T. M., Le, T. V., Do, H. Q., Nguyen, V. T., Holterman, A. X. L., Dang, L. T. T., Phan, N. C. L., Pham, P. V., Hoang, S. N., Le, L. T., Grassi, G., & Truong, N. H. (2021). Optimization of the isolation procedure and culturing conditions for hepatic stellate cells obtained from mouse. *Bioscience Reports*, *41*(1), BSR20202514. https://doi.org/10.1042/BSR20202514

Derbyshire, E. R., & Marletta, M. A. (2012). Structure and regulation of soluble guanylate cyclase. *Annual Review of Biochemistry*, *81*, 533–559. https://doi.org/10.1146/annurev-biochem-050410-100030

Fabre, T., Barron, A. M. S., Christensen, S. M., Asano, S., Bound, K., Lech, M. P., Wadsworth, M. H., Chen, X., Wang, C., Wang, J., McMahon, J., Schlerman, F., White, A., Kravarik, K. M., Fisher, A. J., Borthwick, L. A., Hart, K. M., Henderson, N. C., Wynn, T. A., & Dower, K. (2023). Identification of a broadly fibrogenic macrophage

subset induced by type 3 inflammation. *Science Immunology*, *8*(82), eadd8945. https://doi.org/10.1126/sciimmunol.add8945

Feil, R., & Kemp-Harper, B. (2006). cGMP signalling: From bench to bedside. Conference on cGMP generators, effectors and therapeutic implications. *EMBO Reports*, *7*(2), 149–153. https://doi.org/10.1038/sj.embor.7400627

Feil, R., Lehners, M., Stehle, D., & Feil, S. (2022). Visualising and understanding cGMP signals in the cardiovascular system. *British Journal of Pharmacology*, *179*(11), 2394–2412. https://doi.org/10.1111/bph.15500

Feil, R., Lohmann, S. M., de Jonge, H., Walter, U., & Hofmann, F. (2003). Cyclic GMP-dependent protein kinases and the cardiovascular system: Insights from genetically modified mice. *Circulation Research*, *93*(10), 907–916. https://doi.org/10.1161/01.RES.0000100390.68771.CC

Feng, W., Yang, J., Lei, J., Li, L., Shan, C., Chen, S., Zhang, Z., Zhao, Z., Zhou, S., Zhao, A., Mu, Y., & Li, F. (2025). A novel phosphodiesterase 5 inhibitor, CPD1, alleviates liver fibrosis by modulating the Akt/NF-kappaB pathway to inhibit activated hepatic stellate cells. *Biochemical Pharmacology*, *242*(Pt 3), 117388. https://doi.org/10.1016/j.bcp.2025.117388

Fiebig, T., Boll, H., Figueiredo, G., Kerl, H. U., Nittka, S., Groden, C., Kramer, M., & Brockmann, M. A. (2012). Three-dimensional in vivo imaging of the murine liver: A micro-computed tomography-based anatomical study. *PLoS ONE*, *7*(2), e31179. https://doi.org/10.1371/journal.pone.0031179

Filliol, A., Saito, Y., Nair, A., Dapito, D. H., Yu, L. X., Ravichandra, A., Bhattacharjee, S., Affo, S., Fujiwara, N., Su, H., Sun, Q., Savage, T. M., Wilson-Kanamori, J. R., Caviglia, J. M., Chin, L., Chen, D., Wang, X., Caruso, S., Kang, J. K., … Schwabe, R. F. (2022). Opposing roles of hepatic stellate cell subpopulations in hepatocarcinogenesis. *Nature*, *610*(7931), 356–365. https://doi.org/10.1038/s41586-022-05289-6

Forstermann, U., & Sessa, W. C. (2012). Nitric oxide synthases: Regulation and function. *European Heart Journal*, *33*(7), 829–837, 837a-837d. https://doi.org/10.1093/eurheartj/ehr304

Franko, A., Kovarova, M., Feil, S., Feil, R., Wagner, R., Heni, M., Königsrainer, A., Ruoß, M., Nüssler, A. K., Weigert, C., Häring, H. U., Lutz, S. Z., & Peter, A. (2018). cGMP-dependent protein kinase I (cGKI) modulates human hepatic stellate cell activation. *Metabolism*, *88*, 22–30. https://doi.org/10.1016/j.metabol.2018.09.001

Friebe, A., & Koesling, D. (2003). Regulation of nitric oxide-sensitive guanylyl cyclase. *Circulation Research*, *93*(2), 96–105. https://doi.org/10.1161/01.RES.0000082524.34487.31

Friedman, S. L., Neuschwander-Tetri, B. A., Rinella, M., & Sanyal, A. J. (2018). Mechanisms of NAFLD development and therapeutic strategies. *Nature Medicine*, *24*(7), 908–922. https://doi.org/10.1038/s41591-018-0104-9

Geng, Y., & Schwabe, R. F. (2025). Hepatic stellate cell heterogeneity: Functional aspects and therapeutic implications. *Hepatology*, 10-1097. https://doi.org/10.1097/HEP.0000000000001386

Hagstrom, H., Shang, Y., Hegmar, H., & Nasr, P. (2024). Natural history and progression of metabolic dysfunction-associated steatotic liver disease. *The Lancet Gastroenterology & Hepatology*, *9*(10), 944–956. https://doi.org/10.1016/S2468-1253(24)00193-6

He, W., Huang, C., Shi, X., Wu, M., Li, H., Liu, Q., Zhang, X., Zhao, Y., & Li, X. (2023). Single-cell transcriptomics of hepatic stellate cells uncover crucial pathways and key regulators involved in non-alcoholic steatohepatitis. *Endocrine Connections*, *12*(2), e220502. https://doi.org/10.1530/EC-22-0502

Hofmann, F. (2020). The cGMP system: Components and function. *Biological Chemistry*, *401*(4), 447–469. https://doi.org/10.1515/hsz-2019-0386

Ishak, K., Baptista, A., Bianchi, L., Callea, F., De Groote, J., Gudat, F., Denk, H., Desmet, V., Korb, G., MacSween, R. N., & Phillips, M. J. (1995). Histological grading and staging of chronic hepatitis. *Journal of Hepatology*, *22*(6), 696–699. https://doi.org/10.1016/0168-8278(95)80226-6

Jamialahmadi, O., De Vincentis, A., Tavaglione, F., Malvestiti, F., Li-Gao, R., Mancina, R. M., Alvarez, M., Gelev, K., Maurotti, S., Vespasiani-Gentilucci, U., Rosendaal, F. R., Kozlitina, J., Pajukanta, P., Pattou, F., Valenti, L., & Romeo, S. (2024). Partitioned polygenic risk scores identify distinct types of metabolic dysfunction-associated steatotic liver disease. *Nature Medicine*, *30*(12), 3614–3623. https://doi.org/10.1038/s41591-024-03284-0

Jones, A. K., Chen, H., Ng, K. J., Villalona, J., McHugh, M., Zeveleva, S., Wilks, J., Brilisauer, K., Bretschneider, T., Qian, H. S., & Fryer, R. M. (2023). Soluble guanylyl cyclase activator BI 685509 reduces portal hypertension and portosystemic shunting in a rat thioacetamide-induced cirrhosis model. *The Journal of Pharmacology and Experimental Therapeutics*, *386*(1), 70–79. https://doi.org/10.1124/jpet.122.001532

Kelly, M. P., Nikolaev, V. O., Gobejishvili, L., Lugnier, C., Hesslinger, C., Nickolaus, P., Kass, D. A., de Pereira Vasconcelos, W., Fischmeister, R., Brocke, S., Epstein, P. M., Piazza, G. A., Keeton, A. B., Zhou, G., Abdel-Halim, M., Abadi, A. H., Baillie, G. S., Giembycz, M. A., Bolger, G., … Roks, A. J. M. (2025). Cyclic nucleotide phosphodiesterases as drug targets. *Pharmacological Reviews*, *77*(3), 100042. https://doi.org/10.1016/j.pharmr.2025.100042

Kisseleva, T., & Brenner, D. (2021). Molecular and cellular mechanisms of liver fibrosis and its regression. *Nature Reviews. Gastroenterology & Hepatology*, *18*(3), 151–166. https://doi.org/10.1038/s41575-020-00372-7

Knorr, A., Hirth-Dietrich, C., Alonso-Alija, C., Harter, M., Hahn, M., Keim, Y., Wunder, F., & Stasch, J. P. (2008). Nitric oxide-independent activation of soluble guanylate cyclase by BAY 60-2770 in experimental liver fibrosis. *Arzneimittel-Forschung*, *58*(2), 71–80. https://doi.org/10.1055/s-0031-1296471

Kreisel, W., Lazaro, A., Trebicka, J., Grosse Perdekamp, M., Schmitt-Graeff, A., & Deibert, P. (2021). Cyclic GMP in liver cirrhosis—Role in pathophysiology of portal hypertension and therapeutic implications. *International Journal of Molecular Sciences*, *22*(19), 10372. https://doi.org/10.3390/ijms221910372

Lehners, M., Schmidt, H., Zaldivia, M. T. K., Stehle, D., Kramer, M., Peter, A., Adler, J., Lukowski, R., Feil, S., & Feil, R. (2025). Single-cell analysis identifies the CNP/GC-B/cGMP axis as marker and regulator of modulated VSMCs in atherosclerosis. *Nature Communications*, *16*(1), 429. https://doi.org/10.1038/s41467-024-55687-9

Lilley, E., Stanford, S. C., Kendall, D. E., Alexander, S. P. H., Cirino, G., Docherty, J. R., George, C. H., Insel, P. A., Izzo, A. A., Ji, Y., Panettieri, R. A., Sobey, C. G., Stefanska, B., Stephens, G., Teixeira, M., & Ahluwalia, A. (2020). ARRIVE 2.0 and the British Journal of Pharmacology: Updated guidance for 2020. *British Journal of Pharmacology*, *177*(16), 3611–3616. https://doi.org/10.1111/bph.15178

Lucas, K. A., Pitari, G. M., Kazerounian, S., Ruiz-Stewart, I., Park, J., Schulz, S., Chepenik, K., & Waldman, S. (2000). Guanylyl cyclases and signaling by cyclic GMP. *Pharmacological Reviews*, *52*(3), 375–413.

Lutz, S. Z., Hennige, A. M., Feil, S., Peter, A., Gerling, A., Machann, J., Kröber, S. M., Rath, M., Schürmann, A., Weigert, C., Häring, H. U., & Feil, R. (2011). Genetic ablation of cGMP-dependent protein kinase type I causes liver inflammation and fasting hyperglycemia. *Diabetes*, *60*(5), 1566–1576. https://doi.org/10.2337/db10-0760

Madisen, L., Zwingman, T. A., Sunkin, S. M., Oh, S. W., Zariwala, H. A., Gu, H., Ng, L. L., Palmiter, R. D., Hawrylycz, M. J., Jones, A. R., Lein, E. S., & Zeng, H. (2010). A robust and high-throughput Cre reporting and characterization system for the whole mouse brain. *Nature Neuroscience*, *13*(1), 133–140. https://doi.org/10.1038/nn.2467

Mederacke, I., Dapito, D. H., Affo, S., Uchinami, H., & Schwabe, R. F. (2015). High-yield and high-purity isolation of hepatic stellate cells

from normal and fibrotic mouse livers. *Nature Protocols*, *10*(2), 305–315. https://doi.org/10.1038/nprot.2015.017

Mederacke, I., Hsu, C. C., Troeger, J. S., Huebener, P., Mu, X., Dapito, D. H., Pradere, J. P., & Schwabe, R. F. (2013). Fate tracing reveals hepatic stellate cells as dominant contributors to liver fibrosis independent of its aetiology. *Nature Communications*, *4*, 2823. https://doi.org/10.1038/ncomms3823

Percie, N., Hurst, V., Ahluwalia, A., Alam, S., Avey, M. T., Baker, M., Browne, W. J., Clark, A., Cuthill, I. C., Dirnagl, U., Emerson, M., Garner, P., Holgate, S. T., Howells, D. W., Karp, N. A., Lazic, S. E., Lidster, K., MacCallum, C., Macleod, M., … Würbel, H. (2020). The ARRIVE guidelines 2.0: Updated guidelines for reporting animal research. *BMJ Open Science*, *4*(1), e100115. https://doi.org/10.1136/bmjos-2020-100115

Perez-Ternero, C., Li, W., Aubdool, A. A., Goldin, R. D., Loy, J., Devalia, K., Alazawi, W., & Hobbs, A. J. (2025). Endogenous C-type natriuretic peptide offsets the pathogenesis of steatohepatitis, hepatic fibrosis, and portal hypertension. *PNAS Nexus*, *4*(1), pgae579. https://doi.org/10.1093/pnasnexus/pgae579

Raverdy, V., Tavaglione, F., Chatelain, E., Lassailly, G., De Vincentis, A., Vespasiani-Gentilucci, U., Qadri, S. F., Caiazzo, R., Verkindt, H., Saponaro, C., Kerr-Conte, J., Baud, G., Marciniak, C., Chetboun, M., Oukhouya-Daoud, N., Blanck, S., Vandel, J., Olsson, L., Chakaroun, R., … Pattou, F. (2024). Data-driven cluster analysis identifies distinct types of metabolic dysfunction-associated steatotic liver disease. *Nature Medicine*, *30*(12), 3624–3633. https://doi.org/10.1038/s41591-024-03283-1

Rinella, M. E., Lazarus, J. V., Ratziu, V., Francque, S. M., Sanyal, A. J., Kanwal, F., Romero, D., Abdelmalek, M. F., Anstee, Q. M., Arab, J. P., Arrese, M., Bataller, R., Beuers, U., Boursier, J., Bugianesi, E., Byrne, C. D., Narro, G. E. C., Chowdhury, A., Cortez-Pinto, H., … group, N. N. c. (2024). A multisociety Delphi consensus statement on new fatty liver disease nomenclature. *Annals of Hepatology*, *29*(1), 101133. https://doi.org/10.1016/j.aohep.2023.101133

Routray, C., Liu, C., Yaqoob, U., Billadeau, D. D., Bloch, K. D., Kaibuchi, K., Shah, V. H., & Kang, N. (2011). Protein kinase G signaling disrupts Rac1-dependent focal adhesion assembly in liver specific pericytes. *American Journal of Physiology. Cell Physiology*, *301*(1), C66–C74. https://doi.org/10.1152/ajpcell.00038.2011

Sandner, P., Follmann, M., Becker-Pelster, E., Hahn, M. G., Meier, C., Freitas, C., Roessig, L., & Stasch, J. P. (2021). SolubleGC stimulators and activators: Past, present and future. *British Journal of Pharmacology*, *181*(21), 4130–4151. https://doi.org/10.1111/bph.15698

Schierwagen, R., Maybuchen, L., Zimmer, S., Hittatiya, K., Back, C., Klein, S., Uschner, F. E., Reul, W., Boor, P., Nickenig, G., Strassburg, C. P., Trautwein, C., Plat, J., Lütjohann, D., Sauerbruch, T., Tacke, F., & Trebicka, J. (2015). Seven weeks of Western diet in apolipoprotein-E-deficient mice induce metabolic syndrome and non-alcoholic steatohepatitis with liver fibrosis. *Scientific Reports*, *5*, 12931. https://doi.org/10.1038/srep12931

Schindelin, J., Arganda-Carreras, I., Frise, E., Kaynig, V., Longair, M., Pietzsch, T., Preibisch, S., Rueden, C., Saalfeld, S., Schmid, B., Tinevez, J. Y., White, D. J., Hartenstein, V., Eliceiri, K., Tomancak, P., & Cardona, A. (2012). Fiji: An open-source platform for biological-image analysis. *Nature Methods*, *9*(7), 676–682. https://doi.org/10.1038/nmeth.2019

Schonke, M., & Rensen, P. C. N. (2024). Mouse models for the study of liver fibrosis regression in vivo and ex vivo. *Journal of Clinical and Translational Hepatology*, *12*(11), 930–938. https://doi.org/10.14218/JCTH.2024.00212

Schwabe, R. F., & Brenner, D. A. (2025). Hepatic stellate cells: Balancing homeostasis, hepatoprotection and fibrogenesis in health and disease. *Nature Reviews. Gastroenterology & Hepatology*, *22*(7), 481–499. https://doi.org/10.1038/s41575-025-01068-6

Segnani, C., Ippolito, C., Antonioli, L., Pellegrini, C., Blandizzi, C., Dolfi, A., & Bernardini, N. (2015). Histochemical detection of collagen fibers by sirius red/fast green is more sensitive than van Gieson or sirius red alone in normal and inflamed rat colon. *PLoS ONE*, *10*(12), e0144630. https://doi.org/10.1371/journal.pone.0144630

Sorz-Nechay, T., Brusilovskaya, K., Konigshofer, P., Hofer, B. S., Petrenko, O., Simbrunner, B., Taru, V., Bonitz, K., Horstmeier, H., Zinober, K., Regnat, K., Lackner, C., Trauner, M., Sun, P., Truebenbach, I., Kauschke, S. G., Schwabl, P., & Reiberger, T. (2025). Molecular patterns of the NO-sGC-cGMP pathway in progressive and regressive liver fibrosis models. *Scientific Reports*, *15*(1), 27051. https://doi.org/10.1038/s41598-025-12381-0

Stasch, J. P., Schlossmann, J., & Hocher, B. (2015). Renal effects of soluble guanylate cyclase stimulators and activators: A review of the preclinical evidence. *Current Opinion in Pharmacology*, *21*, 95–104. https://doi.org/10.1016/j.coph.2014.12.014

Stehle, D., Xu, M. Z., Schomber, T., Hahn, M. G., Schweda, F., Feil, S., Kraehling, J. R., Eitner, F., Patzak, A., Sandner, P., Feil, R., & Benardeau, A. (2022). Novel soluble guanylyl cyclase activators increase glomerular cGMP, induce vasodilation and improve blood flow in the murine kidney. *British Journal of Pharmacology*, *179*(11), 2476–2489. https://doi.org/10.1111/bph.15586

Sugimoto, A., Saito, Y., Wang, G., Sun, Q., Yin, C., Lee, K. H., Geng, Y., Rajbhandari, P., Hernandez, C., Steffani, M., Qie, J., Savage, T., Goyal, D. M., Ray, K. C., Neelakantan, T. V., Yin, D., Melms, J., Lehrich, B. M., Yasaka, T. M., … Schwabe, R. F. (2025). Hepatic stellate cells control liver zonation, size and functions via R-spondin 3. *Nature*, *640*(8059), 752–761. https://doi.org/10.1038/s41586-025-08677-w

Suzuki, J., Kaji, K., Nishimura, N., Kubo, T., Tomooka, F., Shibamoto, A., Iwai, S., Tsuji, Y., Fujinaga, Y., Kitagawa, K., Namisaki, T., Akahane, T., & Yoshiji, H. (2023). A combination of an angiotensin II receptor and a neprilysin inhibitor attenuates liver fibrosis by preventing hepatic stellate cell activation. *Biomedicine*, *11*(5), 1295. https://doi.org/10.3390/biomedicines11051295

Tao, J., Mallat, A., Gallois, C., Belmadani, S., Mery, P. F., Nhieu, J. T., Pavoine, C., & Lotersztajn, S. (1999). Biological effects of C-type natriuretic peptide in human myofibroblastic hepatic stellate cells. *The Journal of Biological Chemistry*, *274*(34), 23761–23769. https://doi.org/10.1074/jbc.274.34.23761

Theilig, F., Bostanjoglo, M., Pavenstadt, H., Grupp, C., Holland, G., Slosarek, I., Gressner, A. M., Russwurm, M., Koesling, D., & Bachmann, S. (2001). Cellular distribution and function of soluble guanylyl cyclase in rat kidney and liver. *Journal of the American Society of Nephrology*, *12*(11), 2209–2220. https://doi.org/10.1681/ASN.V12112209

Thunemann, M., Wen, L., Hillenbrand, M., Vachaviolos, A., Feil, S., Ott, T., Han, X., Fukumura, D., Jain, R. K., Russwurm, M., de Wit, C., & Feil, R. (2013). Transgenic mice for cGMP imaging. *Circulation Research*, *113*(4), 365–371. https://doi.org/10.1161/CIRCRESAHA.113.301063

Tsuchida, T., & Friedman, S. L. (2017). Mechanisms of hepatic stellate cell activation. *Nature Reviews. Gastroenterology & Hepatology*, *14*(7), 397–411. https://doi.org/10.1038/nrgastro.2017.38

Valtcheva, N., Nestorov, P., Beck, A., Russwurm, M., Hillenbrand, M., Weinmeister, P., & Feil, R. (2009). The commonly used cGMP-dependent protein kinase type I (cGKI) inhibitor Rp-8-Br-PET-cGMPS can activate cGKI in vitro and in intact cells. *The Journal of Biological Chemistry*, *284*(1), 556–562. https://doi.org/10.1074/jbc.M806161200

Wegener, J. W., Nawrath, H., Wolfsgruber, W., Kuhbandner, S., Werner, C., Hofmann, F., & Feil, R. (2002). cGMP-dependent protein kinase I mediates the negative inotropic effect of cGMP in the murine myocardium. *Circulation Research*, *90*(1), 18–20. https://doi.org/10.1161/hh0102.103222

Weinmeister, P., Lukowski, R., Linder, S., Traidl-Hoffmann, C., Hengst, L., Hofmann, F., & Feil, R. (2008). Cyclic guanosine monophosphate-dependent protein kinase I promotes adhesion of primary vascular smooth muscle cells. *Molecular Biology of the Cell*, *19*(10), 4434–4441. https://doi.org/10.1091/mbc.e08-04-0370

Wiering, L., Subramanian, P., & Hammerich, L. (2023). Hepatic stellate cells: Dictating outcome in nonalcoholic fatty liver disease. *Cellular and Molecular Gastroenterology and Hepatology*, *15*(6), 1277–1292. https://doi.org/10.1016/j.jcmgh.2023.02.010

Wiest, R., & Groszmann, R. J. (2002). The paradox of nitric oxide in cirrhosis and portal hypertension: Too much, not enough. *Hepatology*, *35*(2), 478–491. https://doi.org/10.1053/jhep.2002.31432

Wittrien, T., Ruhle, A., Elgert, C., Mathar, I., Sandner, P., & Behrends, S. (2025). Runcaciguat activates soluble guanylyl cyclase via the histidine essential for heme binding and nitric oxide activation. *Biochemical Pharmacology*, *232*, 116739. https://doi.org/10.1016/j.bcp.2025.116739

Wojcik-Cichy, K., Koslinska-Berkan, E., & Piekarska, A. (2018). The influence of NAFLD on the risk of atherosclerosis and cardiovascular diseases. *Clinical and Experimental Hepatology*, *4*(1), 1–6. https://doi.org/10.5114/ceh.2018.73155

Wolfsgruber, W., Feil, S., Brummer, S., Kuppinger, O., Hofmann, F., & Feil, R. (2003). A proatherogenic role for cGMP-dependent protein kinase in vascular smooth muscle cells. *Proceedings of the National Academy of Sciences of the United States of America*, *100*(23), 13519–13524. https://doi.org/10.1073/pnas.1936024100

Yang, W., He, H., Wang, T., Su, N., Zhang, F., Jiang, K., Zhu, J., Zhang, C., Niu, K., Wang, L., Yuan, X., Liu, N., Li, L., Wei, W., & Hu, J. (2021). Single-cell transcriptomic analysis reveals a hepatic stellate cell-activation roadmap and myofibroblast origin during liver fibrosis in mice. *Hepatology*, *74*(5), 2774–2790. https://doi.org/10.1002/hep.31987

Yokoi, Y., Namihisa, T., Kuroda, H., Komatsu, I., Miyazaki, A., Watanabe, S., & Usui, K. (1984). Immunocytochemical detection of desmin in fat-storing cells (Ito cells). *Hepatology*, *4*(4), 709–714. https://doi.org/10.1002/hep.1840040425

Zhang, S. H., Reddick, R. L., Piedrahita, J. A., & Maeda, N. (1992). Spontaneous hypercholesterolemia and arterial lesions in mice lacking apolipoprotein E. *Science*, *258*(5081), 468–471. https://doi.org/10.1126/science.1411543

Zhao, M., Wang, L., Wang, M., Zhou, S., Lu, Y., Cui, H., Racanelli, A., Zhang, L., Ye, T., Ding, B., Zhang, B., Yang, J., & Yao, Y. (2022). Targeting fibrosis, mechanisms and cilinical trials. *Signal Transduction and Targeted Therapy*, *7*(1), 206. https://doi.org/10.1038/s41392-022-01070-3

How to cite this article: Rajeeth, K., Roessing, M., Lehners, M., Dietz, L., Schmitt, A., Hailfinger, S., Peter, A., Quintanilla-Martinez, L., Gonzalez-Menendez, I., Mederacke, I., Ott, G., Sandner, P., Schwab, M., Feil, R., & Feil, S. (2026). Pharmacological activation of NO-cGMP signalling attenuates metabolic dysfunction-associated steatohepatitis. *British Journal of Pharmacology*, 1–20. https://doi.org/10.1111/bph.70523